Experimental study of organic Rankine cycle in the presence of non-condensable gases

Jing Li[1,2], Guangtao Gao[1], Pengcheng Li[3], Gang Pei[1]*, Hulin Huang[4], Yuehong Su[2], Jie Ji[1]

[1]*Department of Thermal Science and Energy Engineering, University of Science and Technology of China, 96Jinzhai Road,*

Hefei, China

[2]*Department of Architecture and Built Environment, University of Nottingham, University Park, Nottingham NG7 2RD, United*

Kingdom

[3]*School of Automobile and Traffic Engineering, Hefei University of Technology, 193Tunxi Road, Hefei, China*

[4]*School of Energy and Power Engineering, Nanjing University of Aeronautics and Astronautics, 29Jiangjun Road, Nanjing,*

China

*Corresponding author. Tel. /Fax: +86 551 63601652. E-mail: peigang@ustc.edu.cn

Abstract：Non-condensable gases (NCGs) are inevitable in organic Rankine cycle (ORC) system, and they have adverse impacts. A small-scale ORC test platform using scroll expander and R123 was constructed to investigate the NCGs effect. The expander backpressure (i.e. condenser outlet pressure) and electricity output were examined on different conditions of NCGs mass fraction (x_{NCG}), hot side temperature (T_h) and condensation temperature (T_c). Two new parameters, namely reduced coefficient of pressure ratio (RCOPR) and filling ratio of reservoir (FROR), were proposed to reveal the mechanism of ORC performance degradation in the presence of NCGs. The results show that the partial pressure of NCGs (P_{NCG}) in reservoir at work differed from that at static state. Unlike R123, NCGs were blocked by the reservoir and had no access to the pump. The accumulation of NCGs led to unexpected expander backpressure, which could be 0.68 bar higher than the saturation pressure when T_h=140 °C, T_c= 50 °C and x_{NCG}= 1.3%. P_{NCG} generally increased as FROR rose. The FROR changed with T_h, T_c and R123 mass flow rate. The relative increment in electricity output of the ORC with x_{NCG}=1.3% over that with x_{NCG}=12% was significant, and could reach 114% when T_h=100 °C and T_c=50 °C.

Keywords: *organic Rankine cycle; non-condensable gas; filling ratio of reservoir; partial pressure; electricity output.*

Nomenclature

E	electricity output, W	**Subscripts**		
f	frequency, Hz	c	condensation/condenser	
M	mass, kg	e	electricity/evaporation /evaporator	
m	mass flow rate, kg/s	h	hot side	
P	pressure, bar	i	ideal	
T	temperature, ^oC	in	inlet	
V	volume, m^3	l	liquid	
x	mass fraction, %	NCG	non-condensable gas	
ρ	density, kg/m^3	out	outlet	
γ	pressure ratio/ relative change, %	p	organic fluid pump /pressure	

Abbreviation

		res	reservoir
ER	error	$R123$	fluid of R123
$FROR$	filling ratio of reservoir	s	scroll expander
$NCGs$	non-condensable gases	$1.3\%, 12\%$	mass fraction of NCGs
$RCOPR$	reduced coefficient of pressure ratio	γ	relative error

1. Introduction

The organic Rankine cycle (ORC) is an effective way to convert low-medium grade thermal energy into electricity [1]. ORC uses low boiling point organic fluids, and thus can obtain high evaporation pressure at low temperature, compared with steam Rankine cycle. In recent years, researches about ORC are booming [2, 3]. Works on real ORC systems with turbine [4-6], scroll expander [7-9], screw expander [10, 11], piston expander [12] and vane expander [13] have been reported. The performance on different conditions of heat source [11, 13, 14], working fluid [15-17], system configuration [18-20] and operation mode [21, 22] has been examined. However, there are few researches related to non-condensable gases (NCGs), which are unavoidable in ORC system.

NCGs refer to impure gases rather than working fluid vapor, which cannot be condensed in normal operation (so called non-condensable gases). Common NCGs include air and nitrogen. There are four main ways for the existence of NCGs in ORC. First, NCGs permeate the system of improperly sealed pipes and valves. Second, NCGs are produced due to the decomposition of working fluid at high temperature and the corrosion of devices during long-time operation. Third, a few of NCGs remain in system after vacuum-pumping. Fourth, NCGs may infiltrate ORC in the event of replacement and maintenance of components. In addition, silicone oils are favorably used in high temperature applications such as biomass power generation and industrial waste heat recovery [23-26]. The ORC system can be troubled by inward NCGs regarding the low saturation pressure of silicone oils at room temperature. The direct vapor generation ORC applied for solar power production can suffer more from NCGs than

56   traditional ORC system in view of the large area of collectors. It is difficult to guarantee the

57   sealing performance of the system under long-term working conditions [27].

58   The effects of NCGs have been evaluated on the performance of heat pipes [28-30],

59   refrigeration equipment [31, 32], heat pumps [33, 34] and steam-based power plants [35, 36].

60   For heat pipes, the results show that NCGs decrease their thermal conductance, especially at

61   low temperatures and low power levels. Besides, NCGs elevate the steady-state operating

62   temperature and prolong the startup time of heat pipes. For air conditioning or absorption

63   refrigeration systems, NCGs increase condensation temperature and pressure, resulting in

64   additional compressor power consumption and lower cooling capacity. For carbon dioxide

65   trans-critical heat pumps, NCGs affect the phase change of carbon dioxide during expansion

66   process. For steam-based power plants, NCGs reduce the heat transfer and condensation rate

67   of steam in condenser. Aside from the influences on specific systems as mentioned above,

68   NCGs impacts are estimated on the heat and mass transfer during condensation process [37],

69   which may include filmwise condensation [38-40] and dropwise condensation [41-43]. These

70   fundamental studies can also be subdivided into experiments [36, 41, 44] and models [45-47],

71   laminar [38, 45, 48] and turbulent flows [39, 46], tubes [40, 47, 49] and plates [41, 44],

72   horizontal [38, 39, 47] and vertical states [44, 45, 49], steam [36, 44, 49] and organic

73   compounds [50, 51]. In general, NCGs degrade the heat and mass transfer due to the increased

74   resistance.

75   Above all, the reports about the effects of NCGs on ORC system are lacked currently. NCGs

76   are likely to affect the heat transfer in heat exchanger, power conversion of expander and thus

77   the whole system performance. A close examination is needed and valuable. This paper

78   presents an experimental study of the effects of NCGs on the behavior of a scroll expander-

79   driven ORC system. Test results of two levels of NCGs are introduced. The pressure

80   distribution and electricity output of the system are investigated on various conditions of hot

81   side temperature, condensation temperature and pump's input power. Based on the results, the

82   mechanism of the impacts of NCGs is explained and some suggestions are given for better

83   handling of NCGs.

84   **2.   System description**
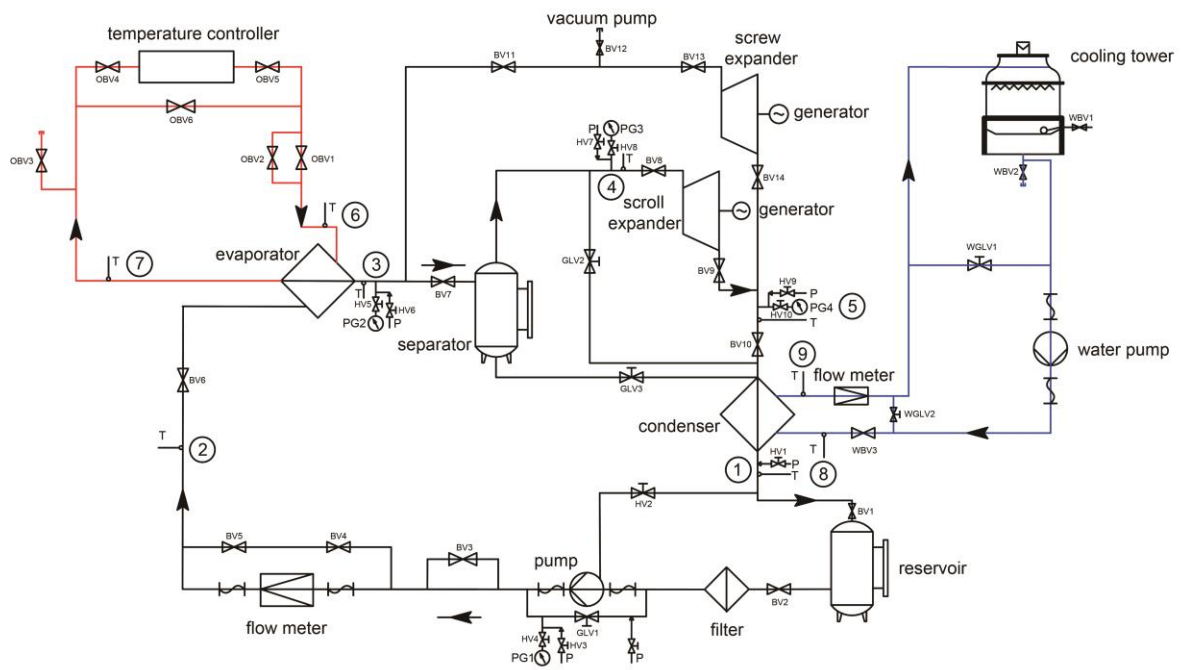
85

86   Fig.1. Structure diagram of the ORC system

87   Fig.1 shows the structure diagram of the ORC system. It contains three subsystems, R123

88   cycle, oil cycle and cooling water cycle. The R123 cycle is depicted as black line, and the oil

89   cycle and the cooling water cycle are represented by red line and blue line. The flow directions

90   of R123, oil and water are denoted by black arrows.

91   The oil was heated to specified temperature in the controller and then transferred the heat to

92   R123 in the evaporator. R123 was vaporized under high pressure. The vapor flew into scroll

93   expander and then exported electricity by the generator due to enthalpy drop. The outlet vapor

94   was condensed into liquid in the condenser, and the heat was taken away by the cooling tower.

95   The liquid was pressurized by the organic fluid pump and sent back to the evaporator. The

96   reservoir was used to store R123 liquid and protect the pump from cavitation. The separator

97   was used to ensure saturated or superheated vapor prior to the expander. The bypasses were

98   used for debugging at the beginning of the experiments and preventing accidents. A screw

99   expander was also involved in the system though not investigated in this paper.

100   The main measure points are shown as numbers 1 to 9 marked with circles in Fig.1. The

101   measured parameters include temperature and pressure, denoted by T and P next to the lines.

102   R123 mass flow rate and electricity output were measured by the flow meter and digital power

103   meter, respectively.

104   The ORC test platform was built on the west campus of the University of Science and

105   Technology of China, Hefei, China. Fig.2a and 2b show the quiescent state and working state,

106   respectively. The high-temperature pipes and components were wrapped with insulation

107   materials to reduce external heat loss (Fig.2a, 2b, 2d). The bulbs dissipated the output

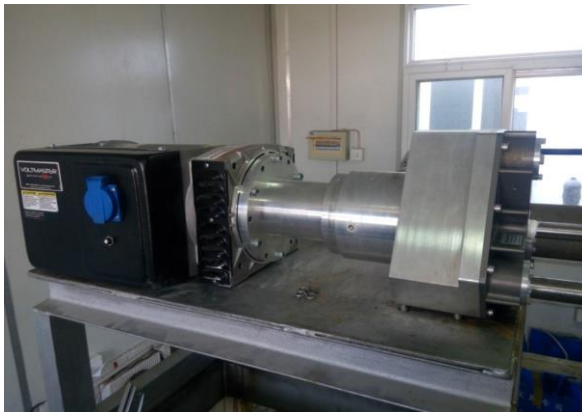108   electricity (Fig.2b), and the nominal power of each bulb was 500 W.

109

110   (a)   (b)

111

112   (c)   (d)

Fig.2. Experiment layout of the ORC system

(a) Quiescent state; (b) Working state; (c) Scroll expander; (d) Reservoir.

The oil-free semi-closed scroll expander was E15H022A-A03 (Fig.2c, Fig.3), provided by

Air Squared, Inc. Its maximum output power, speed, inlet temperature and pressure were 1 kW,

3600 rpm, 175 °C and 13.8 bar, respectively. And the built-in volume ratio was 3.5. The single-

phase generator (AB30L) was produced by Wanco, Inc. It was connected to the expander via a

magnetic coupler in the housing. The rated volts, amps, hertz and speed were 240 V, 10 A, 50

and 3000 rpm.

The evaporator was manufactured by Weal Yield Heat Exchanger Co., Ltd. It consisted of

178 plates, and the heat transfer area was 33.4 m^2. The condenser was fabricated by GEA WTT

123 GmbH. It was made up of 80 plates, and the heat exchange area was 11.31 m^2. Both of them

124 were counter-current plate heat exchangers.

125 The reservoir was designed and manufactured by Hefei General Machinery Research

126 Institute using ICrI8Ni9Ti material (Fig.2d, Fig.4). The total volume was about 33 L, the design

127 pressure and temperature were 1.0 MPa and 10-40 °C.

128 The organic fluid pump (CR1-30) was a centrifugal pump, provided by Grundfos Pumps

129 GmbH. It was driven by an induction motor, located at the top of the pump. The motor was

130 linked with a frequency converter installed on a wall. The R123 mass flow rate and pressure

131 could be regulated by the converter frequency. The cooling water pump (KQL65/110-2.2/2)

132 was a vertical single stage centrifugal pump, and was produced by Shanghai Kaiquan Pump

133 Industry Co., Ltd. The rated flow was 22.3 m^3/h, and the head was 1.6 m. The vacuum pump

134 (2XZ-2) was a rotary vane vacuum pump, and was produced by Linhai Tanshi Vacuum

135 Equipment Co., Ltd. The pumping speed was 2 L/s, the ultimate pressure was 6×10^{-2} Pa, and

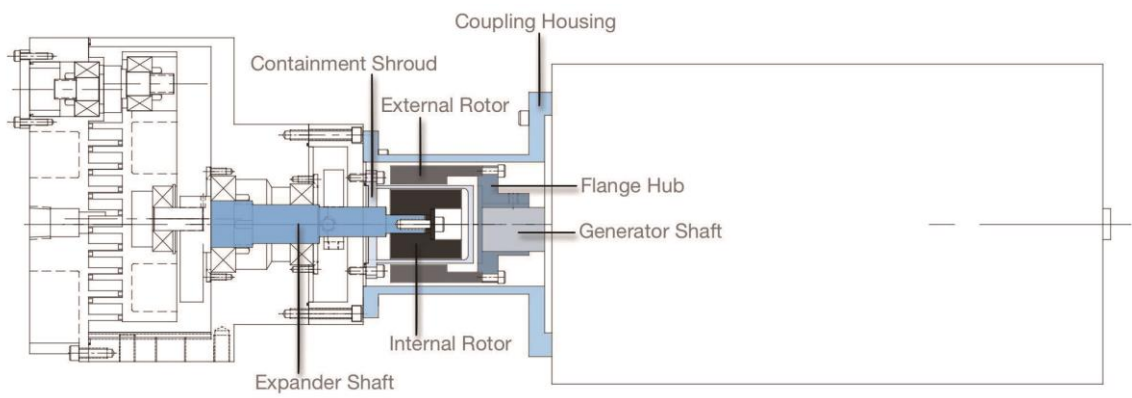136 the motor power was 0.37 kW.

137 The oil temperature controller (AOS-50) was manufactured by Aode Machinery Co. Ltd.

138 The maximum heat output and outlet oil temperature were 100 kW and 200 °C. The cooling

139 tower (ZLT (D) 30) was fabricated by Liyang Global Circulation Cooling Tower Co., Ltd. The

140 volume flow rate of water was 30 m^3/h and the motor power was 1.1 kW.

141
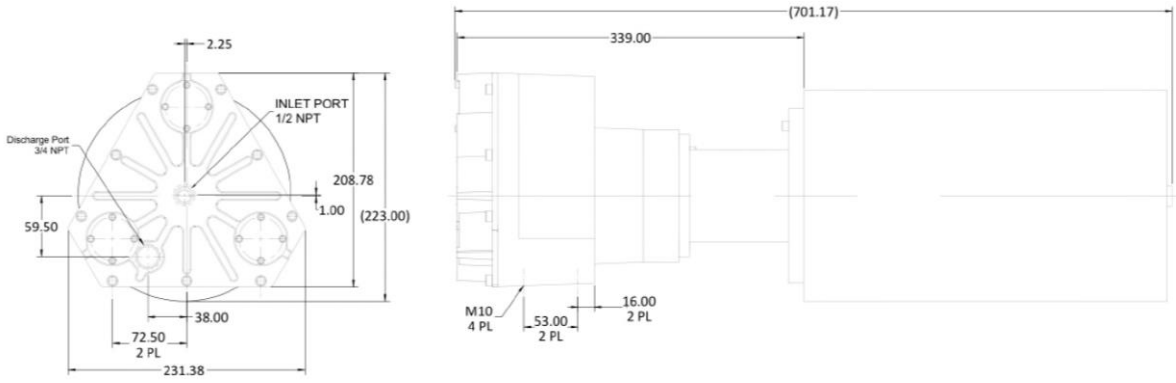
142   (a)

143   E15H022A-SH

144   (b)

145   Fig.3. Structure of the scroll expander-generator unit
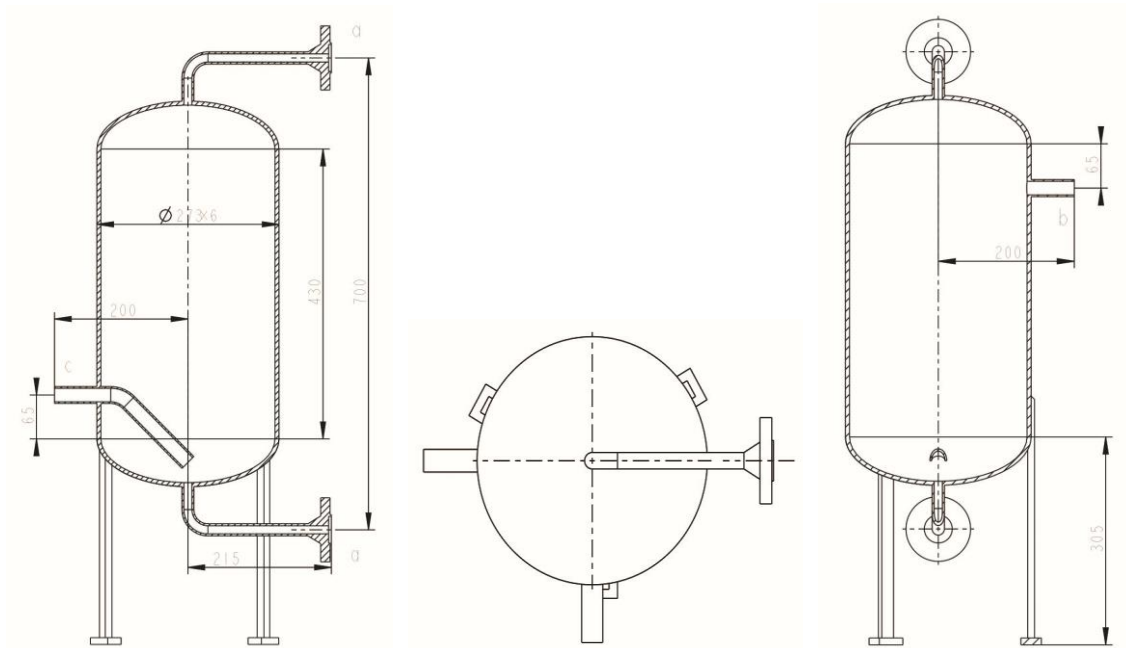
146   (a) End-view; (b) Cutaway view.

147

148   Fig.4. Structure of the reservoir

149   Note: a (Liquidometer interface*2, JB/T82.2-94, WNI5-2.5, Concave); b (Inlet, DN20); c (Outlet, DN20).

150   The temperatures were measured by copper-constantan thermocouples with an accuracy of

151   ±0.5 °C. Three types of ceramic pressure transmitters produced by Huba Control Co. were

152   utilized to measure pressure. The pressure ranges were -1 to 9 bar (scroll expander outlet,

153   condenser outlet and organic fluid pump outlet), 0 to 25 bar (scroll expander inlet) and 0-30

154   bar (organic fluid pump inlet and evaporator outlet). And the accuracies were ±1.0%. The R123

155   mass flow rate was measured by the flow meter (MFM2081K-60P/DN25) fabricated by

156   KROHNE Group. The zero-point stability was ±0.012 kg/min, and accuracy was

157   ±0.15%MV+Cz. The output voltage, current, electricity and frequency of the generator were

158   measured by the digital power meter (8716C1T-RS) provided by Qingdao Qingzhi Company.

159   And the accuracies were ±0.5%, ±0.5%, ±0.5%, and ±0.1%, respectively.

160   The temperature, pressure and mass flow rate data were recorded and stored on disk via a

161 computer data-acquisition system- Agilent 34970A Bench Link Data Logger with a 5-second

162 interval. The output voltage, current, electricity and frequency of the generator were recorded

163 on disk with a 5-second interval by the digital power meter connected with the computer via

164 RS232 interface.

165 **3.   Mathematical models**

166   The static conditions were made to determine the mass fraction of NCGs (x_{NCG}) in the system

167 (Fig.2a). No power was supplied for the devices. There was no mass transfer between the ORC

168 and ambient. Valves at the inlet and outlet of expander, pump, separator, etc., were open. The

169 ORC stayed still for about three days before NCGs measurement was conducted to get

170 approximate thermal equilibrium with the test room. The R123 liquid mainly settled down at

171 the bottom of the system and the vapor/gas accumulated at the upper positions. The R123 vapor

172 and NCGs inside the components kept in touch freely to enable a uniform mixture of them. The

173 solubility of air in most organic solvents was very low [52] and the mass fraction of air in liquid

174 was less than 0.005% at 25 °C and 1.0 bar [53]. Therefore, NCGs that dissolved in the R123

175 liquid were negligible compared with that at gas state.

176   The pressure difference caused by gravity was neglected regarding the small size of the

177 system and low density of the vapor/gas. The total pressure at the vapor/gas regions of the

178 system was the sum of the partial pressures of R123 and NCGs.

$$P = P_{R123} + P_{NCG} \tag{1}$$

180 R123 was at binary phase in the system and P_{R123} was equal to its saturation pressure. The

181   total pressure was measured by pressure transmitters. The partial pressure of NCGs was then

182   calculated by

$$P_{NCG} = P - P_{R123} \tag{2}$$

184   The mass fraction of NCGs was defined as

$$x_{NCG} = \frac{M_{NCG}}{M_{NCG}+M_{R123}} = \frac{\rho_{NCG}}{\rho_{NCG}+\rho_{R123}} \tag{3}$$

186   Notably, M_{R123} is not the overall mass of R123 in the ORC but the mass at vapor state.

187   The density of R123 at saturation state was a function of temperature

$$\rho_{R123} = f(T) \tag{4}$$

189   The density of NCGs was a function of pressure and temperature

$$\rho_{NCG} = g(T, P_{NCG}) \tag{5}$$

191   The reservoir played a vital role on the NCGs. It was employed to guarantee sufficient liquid

192   for the organic fluid pump, which would work improperly or even be damaged in case of

193   vapor/gas. The outlet of reservoir was expected to be always at liquid state. From this viewpoint,

194   NCGs should be blocked by the reservoir. The partial pressure of NCGs was related to the

195   volume of vapor/gas region inside the reservoir. In order to clearly express this effect, the filling

196   ratio of reservoir was established as an indicator

$$FROR = \frac{V_{l,res}}{V_{res}} \tag{6}$$

198   V_{res} and $V_{l,res}$ were the total and liquid volume of the reservoir, respectively. V_{res} was

199   constant for a constructed reservoir while $V_{l,res}$ was variable.

200   There should be a relationship between P_{NCG} and $FROR$ regarding the low pressure

201   of P_{NCG} if the mass of NCGs inside the reservoir was constant

$$P_{NCG}(1 - FROR)V_{res} = RT \qquad (7)$$

203   R was gas constant of the NCGs.

204   The pressure ratio of the expander was defined as

$$\gamma_p = \frac{P_{s,in}}{P_{s,out}} \qquad (8)$$

206   The following sections would show that NCGs finally accumulated in the regions from the

207   expander outlet to the reservoir inlet during working process. The NCGs in the system changed

208   the expander outlet pressure and affected the electricity output. A reduced coefficient of

209   pressure ratio is proposed

$$RCOPR = \frac{\gamma_{p,i}}{\gamma_p} \qquad (9)$$

211    $\gamma_{p,i}$ was the pressure ratio without NCGs (ideal case), achieved when the expander outlet

212   pressure was equal to the fluid saturation pressure at condensation temperature. A larger

213   RCOPR meant more appreciable impact of NCGs on practical pressure ratio of the expander.

214   The relative change of the electricity output was defined as

$$\gamma_e = \frac{E_{1.3\%} - E_{12\%}}{E_{12\%}} \times 100\% \qquad (10)$$

4. Experiment arrangements

217   The whole experiments fell into two categories. The first one was at x_{NCG} of 12%, and the

218   second one was at x_{NCG} of 1.3%. Each category contained 9 different conditions. The hot side

219   temperatures (T_h) were 100, 120, 140 °C and the condensation temperatures (T_c) were 20, 40

220   and 50 °C, respectively (3×3). Under each condition, R123 mass flow rate and inlet pressure

221   of the scroll expander could be changed by the frequency of the converter.

222   For the higher x_{NCG}, the NCGs came into the system due to the maintenance and replacement

223   of the expander. Generally, R123 and NCGs should have been drained off before these actions

224   and the ORC should have been evacuated by the vacuum pump when the replacement was

225   completed, followed by refilling the organic fluid. The procedures were not conducted in order

226   to investigate the NCGs. R123 decomposed above 250 °C [54], which hardly happened in the

227   experiments because the maximum temperature was only 140 °C. R123 barely corroded

228   components due to its stability [54]. The ORC system had never been filled with other gases.

229   Therefore, the NCGs inside the system were speculated to be air.

230   The variations of temperature and pressure at the expander outlet are presented in Fig.5 on

231   static equilibrium system condition of larger x_{NCG}. The expander was located at a higher

232   position than the condenser, and no liquid at its outlet had been observed at the non-working

233   state. The mass fraction of NCGs was around 12% with a partial pressure of about 0.4 bar,

234   calculated by Eq.(2) and (3).

235   Notably, given the mass of NCGs in the ORC, x_{NCG} is unlikely to be constant and shall

236   increase as the outlet temperature of the scroll expander decreases. The reason is some of the

237   R123 vapor will condense into liquid. During the condensation, the total volume of vapor/gas

238   region should be nearly unvaried in regard to the large density difference between the saturation

239   liquid and vapor of R123. For instance, the former and the latter are 1496.7 and 3.6 kg/m^3 at

240   12 °C. The condensation will lead to decrement in the mass of R123 vapor and increment in

241   x_{NCG}.

242   Fig.6 shows the variations in the case of lower x_{NCG}. A small amount of NCGs was added

243   into the ORC of pure R123 through the valve of vacuum pump. The mass fraction and partial

244   pressure of NCGs were close to 1.3% and 0.1 bar, respectively. In both situations (x_{NCG}=12%

245   and 1.3%), experimental tests were carried out in the absence of mass transfer between the

246   ORC and the ambient.
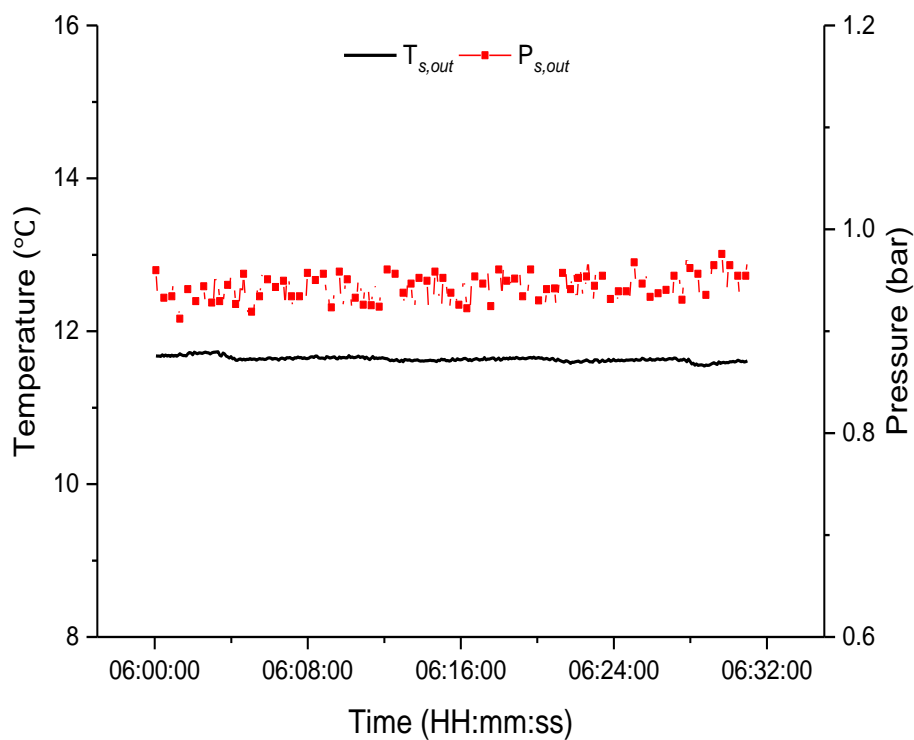
247

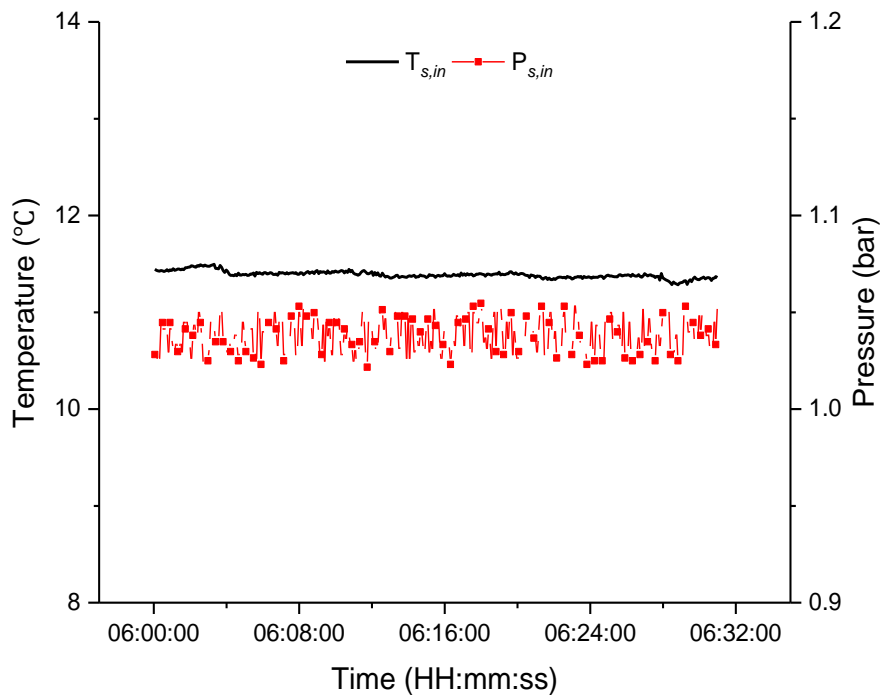248   Fig.5.Variations of temperature and pressure at the scroll expander outlet in the situation of higher x_{NCG}
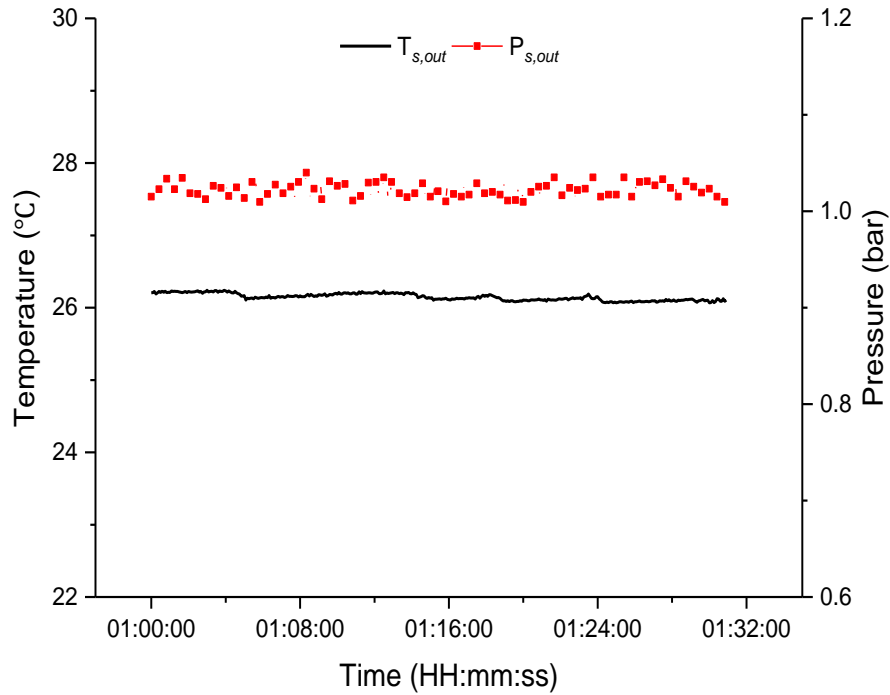
249

250   Fig.6.Variations of temperature and pressure at the scroll expander outlet in the situation of lower x_{NCG}

251 **5.   Results and discussion**

252 *5.1 Mass transfer of NCGs*

253   Quasi-steady temperature and pressure at the expander outlet for the non-running system

254 have been depicted in Section 4. Similar temperature and pressure distributions at the expander

255 inlet (i.e. evaporator outlet) are shown in Fig.7. The estimated partial pressure of NCGs (P_{NCG})

256 was also about 0.4-0.5 bar. So P_{NCG} in the vapor/gas regions was almost uniform when the

257 system was static. However, the distribution of NCGs would be changed when the system

258 shifted to working mode, as discussed below.

259

Fig.7.Variations of temperature and pressure at the scroll expander inlet in the situation of higher x_{NCG}

Fig.8 shows the variations of temperature and pressure at the expander inlet and the condenser outlet for the operating system. T_h was 100 °C (i.e. the thermal oil temperature at the evaporator inlet). The inlet temperature of the expander rose from 85 °C to about 95 °C finally. The fluid temperature at the condenser outlet was relatively steady, fluctuating around 20 °C. The expander inlet pressure climbed from 5.0 bar to 7.6 bar step by step through the adjustment of the converter frequency. According to the thermodynamic properties of R123, the inlet fluid changed from superheated state to almost saturated state at the expander inlet. Unlike the static state with a NCGs partial pressure of about 0.4-0.5 bar, no evidence showed that NCGs existed at the expander inlet in the normal operation of the ORC system.

The reason behind this phenomenon is that NCGs were blocked in the reservoir. NCGs were not able to pass the reservoir when the ORC system worked. The fluid leaving the organic fluid

272   pump was high-purity R123. It continuously went through the evaporator, expander and pipes.

273   Then the NCGs in the evaporator and expander were carried away gradually and squeezed

274   inside the reservoir.

275   It should be pointed out that there was a warm-up process, which was dynamic and lasted

276   for about half an hour, prior to the electricity generation of the ORC system. The thermal oil

277   was slowly heated from the ambient temperature to 100 °C. The temperature and pressure of

278   R123 in the evaporator went up as the oil temperature increased. Then the high-pressure

279   vapor/gas flowed into the condenser where the pressure was low. Mass transfer of NCGs had

280   actually taken place before the expander and organic fluid pump started to run. Fig.8 shows the

281   results when the oil temperature had already reached 100 °C and the expander and pump had

282   functioned. Therefore, most of the NCGs had accumulated in the reservoir even at the

283   beginning (0:00).

284   The fluid pressure at the condenser outlet was decreased (Fig.8). The saturation pressure of

285   R123 in the reservoir should keep approximately constant because the condenser outlet

286   temperature varied slightly. The reduction in the condenser's outlet pressure was due to the

287   decrement in the partial pressure of NCGs (P_{NCG}). Given amount of NCGs in the reservoir,

288   P_{NCG} was expected to be proportional to the FROR. When the pump power was elevated, the

289   mass flow rate of R123 was enlarged. Fluids inside the evaporator became more, resulted in

290   less mass in the reservoir. The FROR and P_{NCG} were hence decreased. As seen from Fig.8, the

291   increment of the expander inlet pressure and the decrement in the condenser outlet pressure

292   occurred nearly simultaneously.
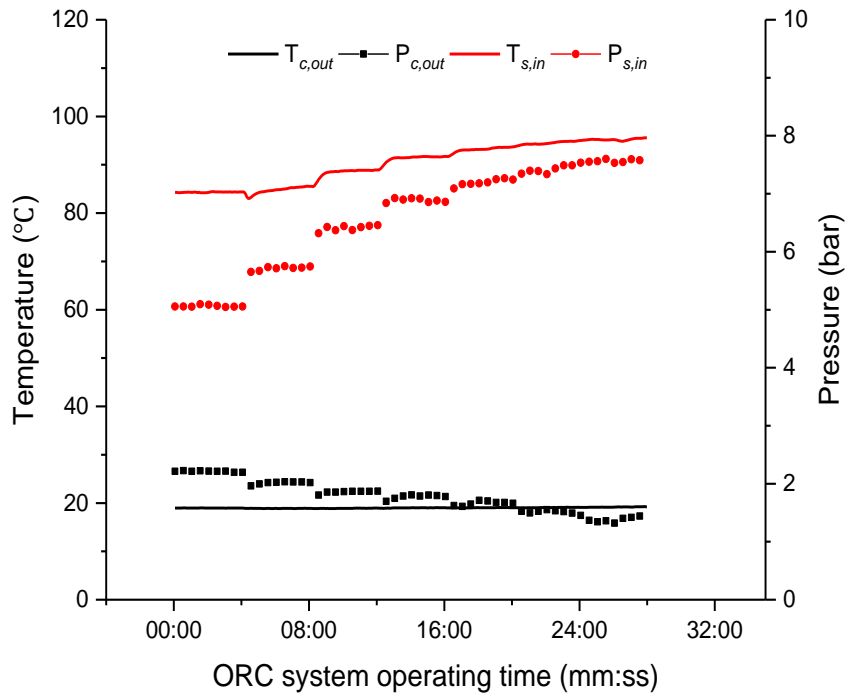
Fig.8. Variations of temperature and pressure at the expander inlet and the condenser outlet on the

conditions of higher x_{NCG} when T_h=100 °C and T_c=20 °C

5.2 The condenser outlet pressure on different operating conditions

Fig.9 shows the variations of condenser outlet pressure. For each curve, T_h, T_c and x_{NCG} were

the same, and only the organic fluid pump's input power was adjusted via the frequency of the

converter with a 4-minute interval. The frequency (*f*) was 18.5 to 21.0, 23.5, 26.0 and 28.5 Hz

in case of T_h=100 °C. At 28.5 Hz, R123 fluid at the evaporator outlet was very close to

saturation state. If the frequency increased further, the evaporation pressure would not rise

while the mass flow rate of R123 would increase dramatically. This would cause emptiness of

the reservoir (no liquid) and cavitation of the organic fluid pump. Hence, the frequency

adjustment would cease when R123 at the evaporator outlet was approaching to saturation state.

In case of T_h=120 °C, the frequency was 18.5 to 21.0, 23.5, 26.0, 28.5, 31.0, 32.0, 33.0, 34.0

306   and 35.0 Hz. And it was 18.5 to 21.0, 23.5, 26.0, 28.5, 31.0, 32.0, 33.0, 34.0, 35.0 and 36 .0 Hz

307   when T_h=140 °C. Though the R123 vapor was still superheated at the evaporator outlet when

308   f=36.0 Hz, the evaporation temperature was close to 13.8 bar, which was the maximum

309   allowable operating pressure of the expander.

310   The variations for all curves are similar in Fig.9. The condenser outlet pressure was generally

311   reduced step by step with the increment in the frequency. This phenomenon was more evident

312   when the system contained more NCGs (x_{NCG} =12%). The decrement of the condenser outlet

313   pressure reached as much as 1.8 bar from the beginning to the end of experiment at T_h=140 °C,

314   T_c=50 °C and x_{NCG} =12%, while it was less than 0.6 bar at x_{NCG} =1.3%. Besides, for each curve

315   the decrement was less appreciable at higher frequency. There are two main reasons. First, the

316   derivative of P_{NCG} with respect to FROR ($d\,P_{NCG}/dFROR$) was $RT/V_{res}(1 - FROR)^{-2}$, and

317   it declined with the decrement in FROR. Second, FROR changed smoothly with the converter

318   frequency (f), and |ΔFROR| was approximately proportional to |Δf|, as observed in the

319   experiments.

320   The step-like drop of the condenser outlet pressure was resulted from the increment in the

321   pump's input power. As mentioned in Section 5.1, the NCGs assembled in the reservoir when

322   the system was operating. A larger pump's input power was accompanied by a higher R123

323   mass flow rate at the evaporator inlet. Then the heat transfer area for liquid and binary phase

324   was enlarged, and the region of high density fluid was extended. Consequently, the total mass

325   inside the evaporator became more. This was also applicable for the condenser. According to

326   the law of mass conservation for the entire cycle, the mass inside the reservoir fell down,

327   accompanied by lower the liquid level and FROR. Take T_h=140 °C, T_c=50 °C and x_{NCG} =12%

328   for example, the initial FROR was close to 90%. While it turned to about 40% when f=36.0 Hz.

329   Since the condensation temperature fluctuated slightly, the partial pressure of NCGs was a

330   monotonically increasing function of FROR in view of the ideal gas Eq.(7).

331   Given the T_c, x_{NCG} and converter frequency, the condenser outlet pressure varied with T_h. At

332   each T_h, the liquid level in the reservoir was different. Higher T_h could lead to larger

333   temperature difference between the oil and R123 in the liquid and binary regions. The heat

334   transfer area for the vaporization of R123 was reduced and the fluid became less in the

335   evaporator (more fluid in the reservoir). Therefore, FROR was an increasing function with

336   respect to the evaporation temperature.

337   Several rebound points of the condenser outlet pressure exist in Fig.9. The condenser outlet

338   pressure declined dramatically after each adjustment of the converter frequency, and it would

339   go up a bit when reaching the lowest value. The 'V'-shape fluctuation could be explained based

340   on the characteristics of the organic fluid pump. In the dynamic process triggered by the

341   adjustment of the converter frequency, the mass flow rate at the evaporator inlet ($m_{e,in}$) differed

342   from that at its outlet ($m_{e,out}$). $m_{e,in}$ was equal to the mass flow rate through the organic fluid

343   pump and was related with the pump's input power, evaporation pressure (P_e) and condensation

344   pressure (P_c). While $m_{e,out}$ was mainly determined by P_e and P_c. A larger difference between P_e

345   and P_c would bring a higher $m_{e,out}$ but a lower $m_{e,in}$. First, the increment in the converter

346   frequency caused a higher pump's input power. Given inlet and outlet pressure of the pump, a

347   sudden acceleration in $m_{e,in}$ was resulted. So at the time of adjustment of the pump's input

348   power, $m_{e,in} > m_{e,out}$. The liquid flowing into the evaporator was more than the vapor leaving it.

349   Hence, much more liquid accumulated in the evaporator and FROR dropped simultaneously.

350   On the other hand, the sudden addition of fluid facilitated a fast increment in the evaporator

351   pressure. As a result, $m_{e,in}$ decreased and $m_{e,out}$ increased. FROR then grew. Eventually a steady

352   state was reached when $m_{e,in}=m_{e,out}$. The balance between $m_{e,in}$ and $m_{e,out}$ would be broken when

353   the converter was further adjusted.
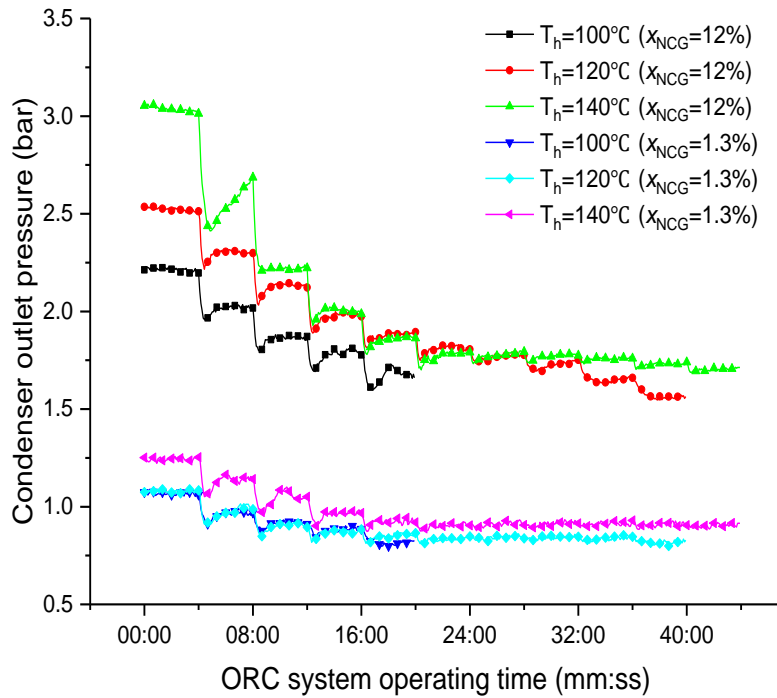
354

355   (a)

356

357

(b)

358

359

(c)

360
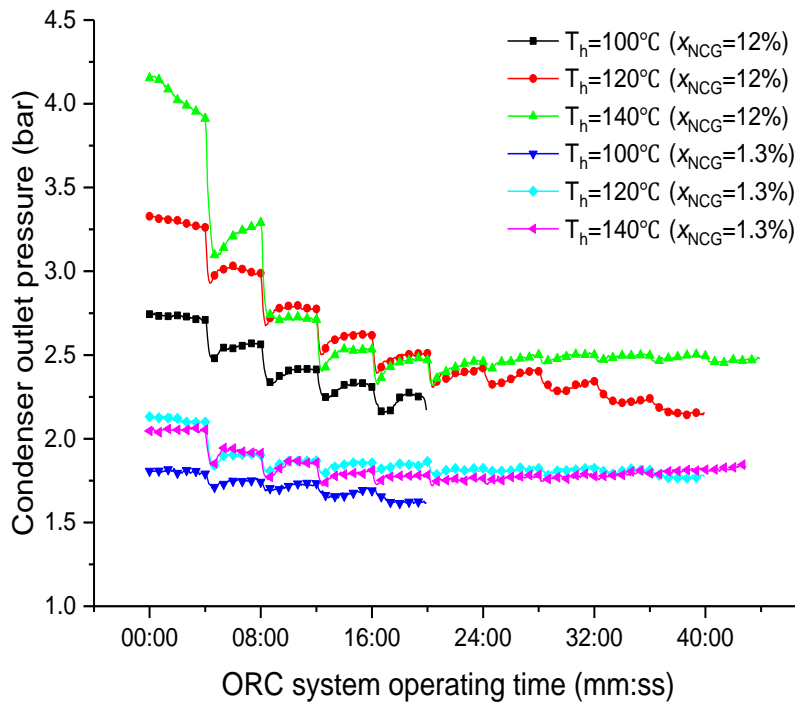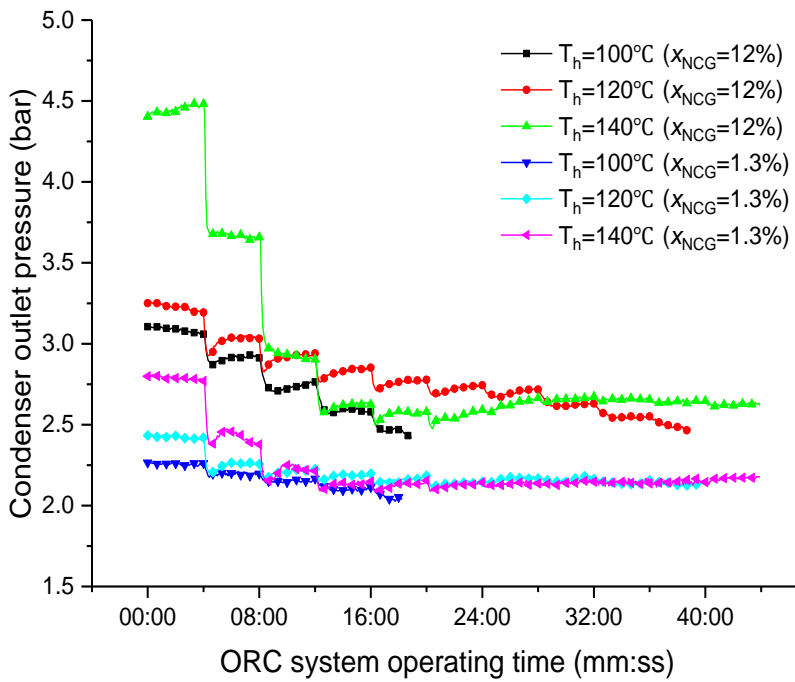
Fig.9. Variations of condenser outlet pressure

361

(a) $T_c=20\ ^\circ C$; (b) $T_c=40\ ^\circ C$; (c) $T_c=50\ ^\circ C$.

362   Fig.10 shows the variations of expander inlet pressure with time. Although the influence of

363   NCGs on the expander inlet pressure was not so remarkable as on the condenser outlet pressure,

364   higher mass fraction of NCGs still led to higher expander inlet pressure at fixed T_h, T_c and

365   converter frequency. The increment was around 1.0 bar. Explanations on the increment can be

366   made in theory. Given the scroll expander speed and the organic fluid pump's input power, the

367   mass flow rates through the expander and the pump are functions of P_e and P_c, as expressed by

368   m_s (P_e, P_c) and m_p (P_e, P_c), respectively. For a steady ORC, mass flow rate is constant, and m_s

369   (P_e, P_c) = m_p (P_e, P_c). This equation establishes the relationship between P_e and P_c.

370   Because

$$(\frac{\partial m_s}{\partial P_c})_{P_e} + (\frac{\partial m_s}{\partial P_e})_{P_c} \cdot \frac{dP_e}{dP_c} = (\frac{\partial m_p}{\partial P_c})_{P_e} + (\frac{\partial m_p}{\partial P_e})_{P_c} \cdot \frac{dP_e}{dP_c} \tag{11}$$

372   Therefore,

$$[(\frac{\partial m_s}{\partial P_e})_{P_c} - (\frac{\partial m_p}{\partial P_e})_{P_c}] \cdot \frac{dP_e}{dP_c} = [(\frac{\partial m_p}{\partial P_c})_{P_e} - (\frac{\partial m_s}{\partial P_c})_{P_e}] \tag{12}$$

374   Because

$$(\frac{\partial m_s}{\partial P_e})_{P_c} > 0 \tag{13}$$

$$(\frac{\partial m_p}{\partial P_e})_{P_c} < 0 \tag{14}$$

$$(\frac{\partial m_p}{\partial P_c})_{P_e} > 0 \tag{15}$$

$$(\frac{\partial m_s}{\partial P_c})_{P_e} < 0 \tag{16}$$

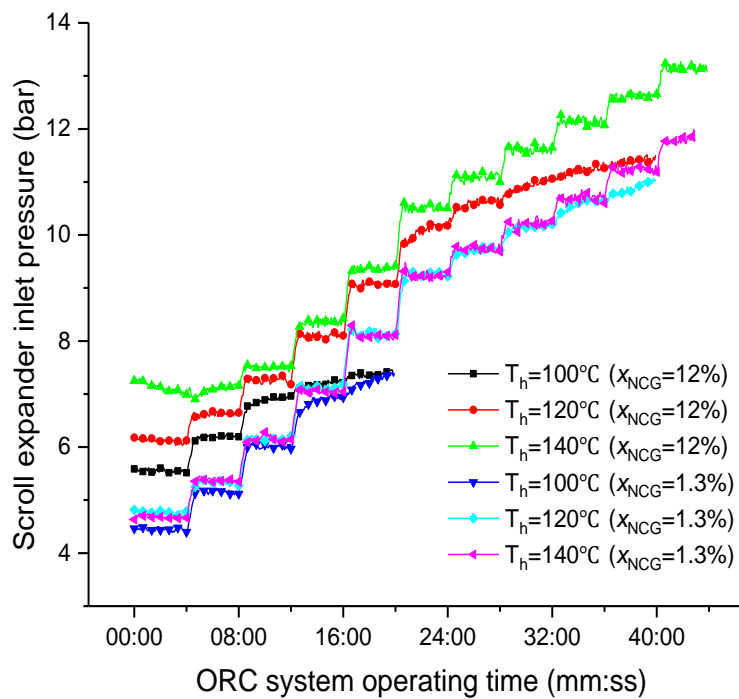379   Therefore

$$\frac{dP_e}{dP_c} > 0 \tag{17}$$

381   Since the condensation pressure of ORC with higher x_{NCG} is larger, the evaporation pressure

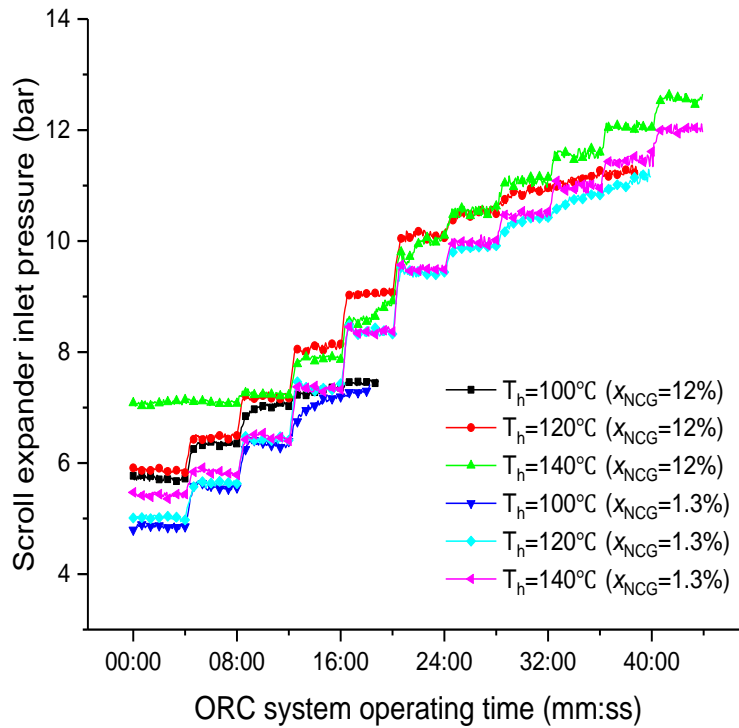382   together with the expander inlet pressure should be higher.
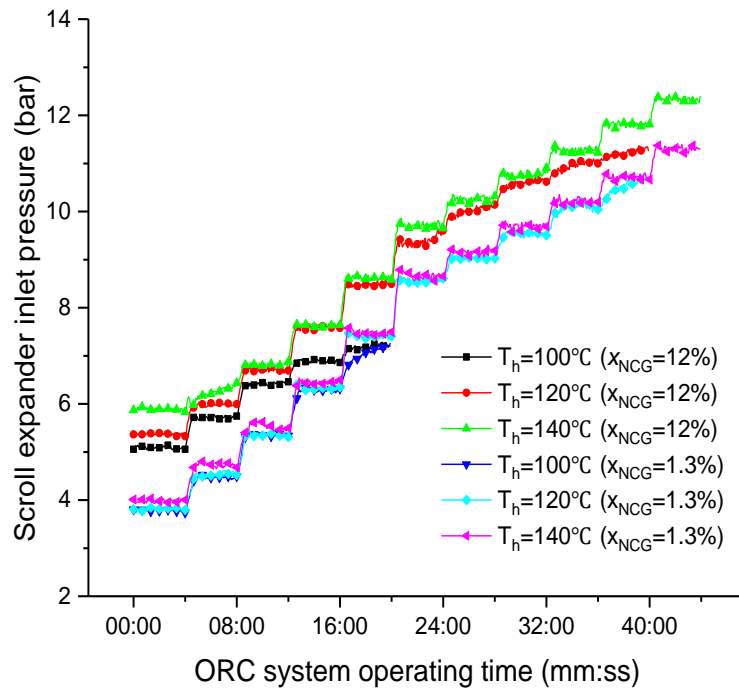
383

384

(a)

385

386

(b)

(c)

Fig.10. Variations of scroll expander inlet pressure

(a) T_c=20 °C; (b) T_c=40 °C; (c) T_c=50 °C.

The variations of the reduced coefficient of pressure ratio (RCOPR) are displayed in Fig.11. The pressure ratio of the expander is an important parameter in practical ORC system. RCOPR was linked with the FROR. For x_{NCG}=12%, RCOPR reached as high as 4.25 at T_h=140 °C, T_c=20 °C and f=18.5 Hz. Given the expander's inlet conditions, reduction in the pressure ratio meant less driving force of power conversion, attributed to the increment in the equivalent condensation temperature. A RCOPR of 3 at T_h=140 °C, T_c=20 °C indicated a backpressure of 2.27 bar, with a corresponding saturation temperature of 52.1 °C. The equivalent condensation temperature exceeded the actual condensation temperature by about 32.1 °C.

From the above results, it is obvious that the presence of NCGs had significant impact on

400   the condensation pressure and thus on the backpressure of the expander even if the mass

401   fraction was low at static state. For example, when $x_{NCG} = 1.3\%$ and $T_h = 140$ °C, the initial

402   condenser outlet pressure was 1.2, 2.0 and 2.8 bar at $T_c = 20$, 40 and 50 °C, higher than the

403   saturation pressure by about 0.44, 0.46 and 0.68 bar, respectively. The distribution of NCGs

404   during the operation of ORC was distinguishable from that at static state. For the former, NCGs

405   were squeezed in a small space in the reservoir. Depending on the FROR, the partial pressure

406   of NCGs could be increased by 10 times or more under the working conditions.
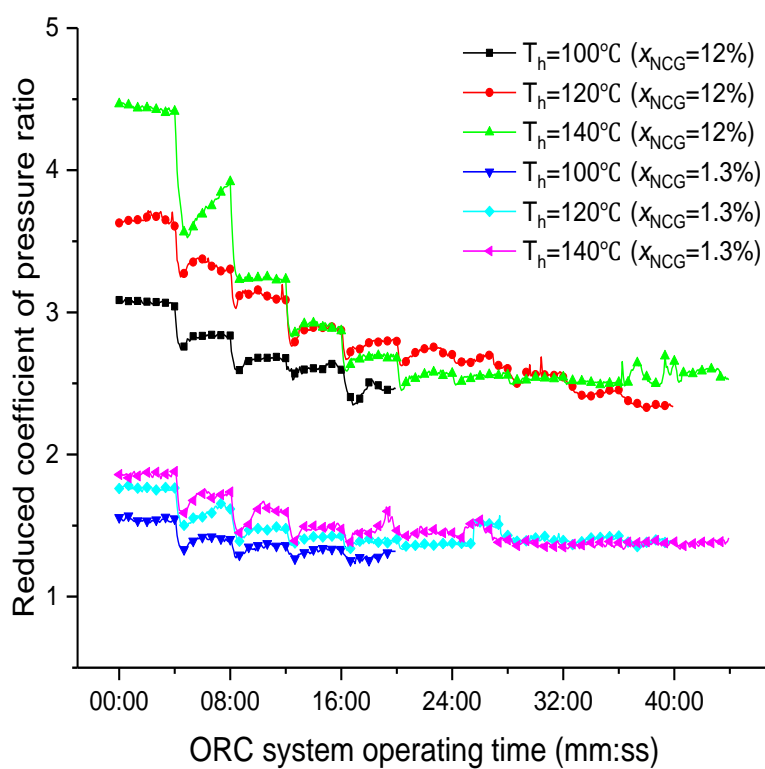
407

408   (a)
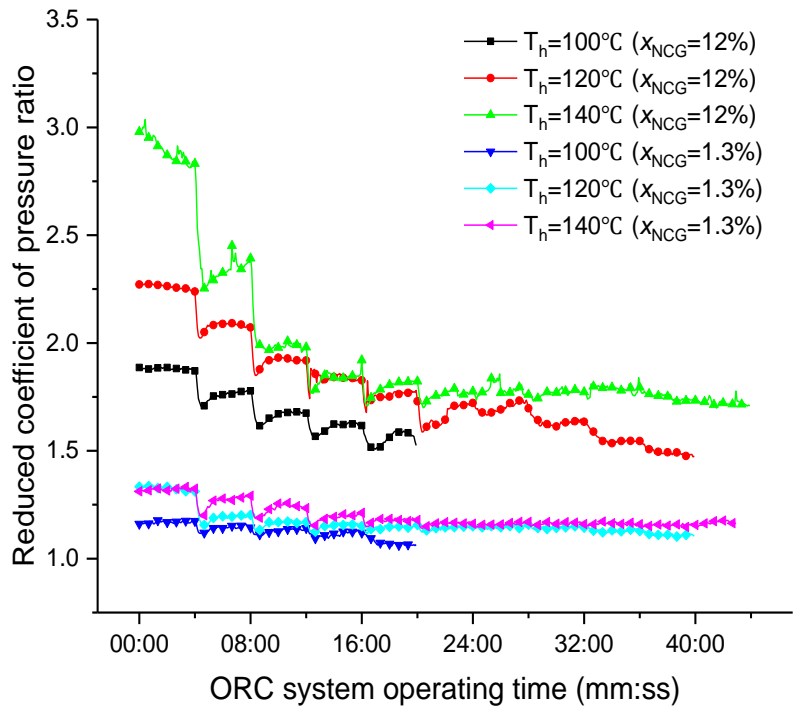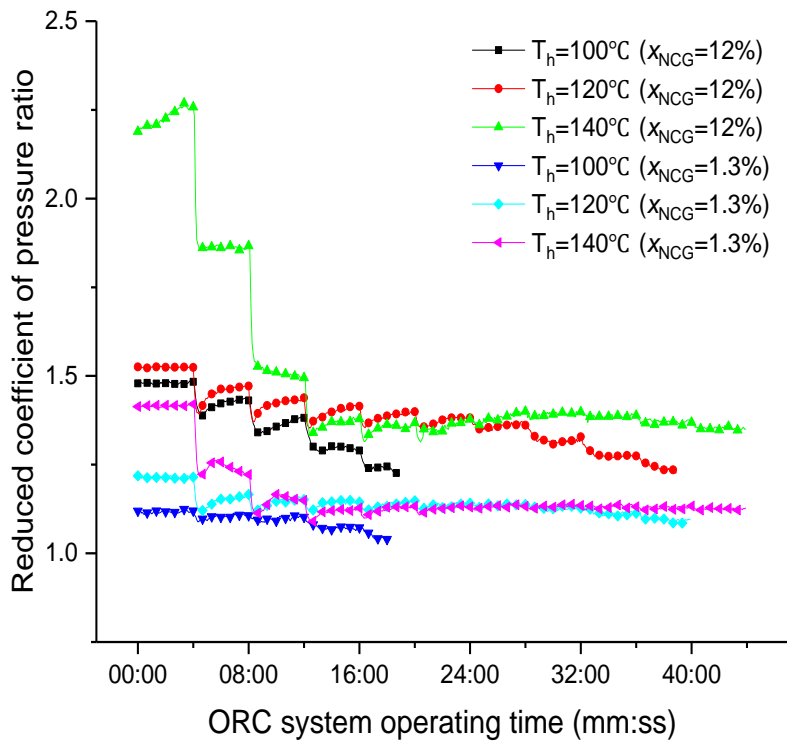
409

410   (b)

411

412   (c)

413   Fig.11. Variations of the reduced coefficient of pressure ratio

414   (a) T_c=20 °C; (b) T_c=40 °C; (c) T_c=50 °C.

5.3 Electricity output of the ORC

416   Table 1 and Table 2 list the electricity output of the ORC system under different operating

417 conditions. ΔE is the difference between the final electricity output and the initial. The

418 rotation speed of the expander is provided in Table 3 and Table 4.

419   The electricity output increased with the increment in the input power of organic fluid pump.

420 As the frequency of the converter climbed, the condenser outlet pressure decreased (Fig.9) and

421 the evaporation pressure increased (Fig.10), leading to a larger operating pressure ratio. Besides,

422 R123 mass flow rate also went up, as shown in Fig.12. As a result, the expander produced more

423 electricity.

424   At the same x_{NCG}, T_c and converter frequency, the electricity output varied slightly with T_h

425 (excluding saturated conditions), attributed to the relatively smooth variation of the evaporation

426 pressure. For example, when x_{NCG}=12%, T_c=20 ℃ and f=18.5 Hz, the evaporation pressures

427 were 5.1, 5.4 and 5.9 bar at T_h=100, 120, 140 ℃, respectively. Due to the sufficient heat transfer

428 area of the evaporator, the outlet temperature of R123 was close to T_h. So, the degree of

429 superheat of R123 at the evaporator outlet increased as T_h climbed.

430   Table 1. Average electricity output when x_{NCG}=12%

f (Hz)	T_c/T_h (℃/℃)								
	20/100	20/120	20/140	40/100	40/120	40/140	50/100	50/120	50/140
18.5	91.0	85.2	78.1	71.8	64.5	56.7	37.7	60.8	50.3

21.0	151.8	144.2	140.4	129.0	120.2	117.3	93.7	112.7	104.8
23.5	212.3	212.0	203.9	184.7	179.1	186.1	153.8	167.4	174.5
26.0	242.3	280.6	275.4	210.9	248.3	260.8	181.2	223.7	243.4
28.5	269.1	344.6	368.0	225.8	311.8	328.4	194.9	292.0	302.0
31.0		406.4	450.3		395.3	419.7		372.8	385.5
32.0		455.3	484.5		435.3	453.2		413.8	424.9
33.0		483.7	521.7		466.5	484.4		449.2	456.1
34.0		514.5	551.0		499.1	520.9		479.5	496.5
35.0		548.3	586.8		523.4	555.8		499.3	529.5
36.0			616.3			592.3			565.9
ΔE	178.1	463.1	538.2	154.0	458.9	535.6	157.2	438.5	515.6

Table 2. Average electricity output when x_{NCG}=1.3%

f (Hz)	T_c/T_h (°C/°C)								
	20/100	**20/120**	**20/140**	**40/100**	**40/120**	**40/140**	**50/100**	**50/120**	**50/140**
18.5	117.4	118.5	117.5	91.8	90.8	87.6	74.4	77.4	75.1
21.0	167.5	173.3	173.0	143.8	148.9	144.4	126.6	132.5	133.3
23.5	219.1	230.2	227.2	202.0	204.2	200.5	183.2	189.7	190.7
26.0	271.8	286.3	289.4	258.8	270.2	260.3	233.0	254.1	254.6
28.5	330.9	363.5	372.1	290.0	332.9	337.6	253.5	319.5	319.6
31.0		438.8	452.5		418.5	422.0		389.7	386.3

f (Hz)	20/100	20/120	20/140	40/100	40/120	40/140	50/100	50/120	50/140
32.0		467.9	485.4		445.8	461.6		422.6	427.8
33.0		493.4	521.0		474.6	497.5		459.6	475.0
34.0		515.1	552.0		501.4	528.7		482.9	515.7
35.0		541.8	583.5		528.7	563.6		496.3	553.1
36.0			617.2			591.7			594.9
ΔE	213.5	423.3	499.7	198.2	437.9	504.1	179.1	418.9	519.8

432　　　　　　　Table 3. Average rotation speed of the scroll expander when $x_{NCG}=12\%$

f (Hz)	T_c/T_h (°C/°C)								
	20/100	20/120	20/140	40/100	40/120	40/140	50/100	50/120	50/140
18.5	1754	1747	1747	1748	1743	1668	1675	1678	1674
21.0	1797	1789	1787	1780	1776	1708	1692	1714	1707
23.5	1873	1872	1861	1832	1830	1799	1758	1786	1789
26.0	1923	1995	1986	1871	1942	1928	1798	1882	1907
28.5	1972	2126	2177	1896	2084	2059	1818	2016	2018
31.0		2262	2352		2206	2246		2184	2188
32.0		2362	2423		2312	2315		2230	2271
33.0		2418	2498		2404	2380		2306	2336
34.0		2483	2557		2463	2453		2358	2418
35.0		2548	2627		2508	2522		2399	2484
36.0			2684			2592			2556

433　　　　　　　Table 4. Average rotation speed of the scroll expander when $x_{NCG}=1.3\%$

f (Hz)	T_c/T_h (°C/°C)								
	20/100	20/120	20/140	40/100	40/120	40/140	50/100	50/120	50/140
18.5	1730	1731	1708	1704	1704	1703	1697	1698	1702
21.0	1791	1800	1773	1757	1760	1757	1738	1746	1748
23.5	1878	1899	1861	1846	1846	1844	1817	1827	1830
26.0	1976	2002	1990	1945	1967	1953	1903	1944	1944
28.5	2078	2161	2177	2005	2091	2105	1941	2070	2070
31.0		2316	2352		2270	2281		2215	2208
32.0		2379	2423		2329	2362		2284	2300
33.0		2431	2497		2390	2436		2368	2395
34.0		2477	2558		2448	2499		2413	2478
35.0		2525	2621		2493	2569		2435	2553
36.0			2686			2624			2635
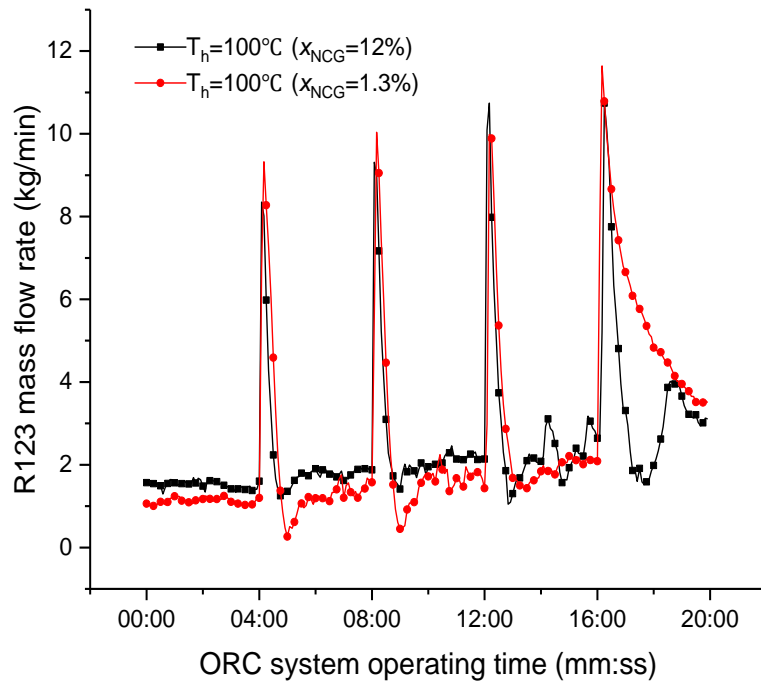
434

435

(a)
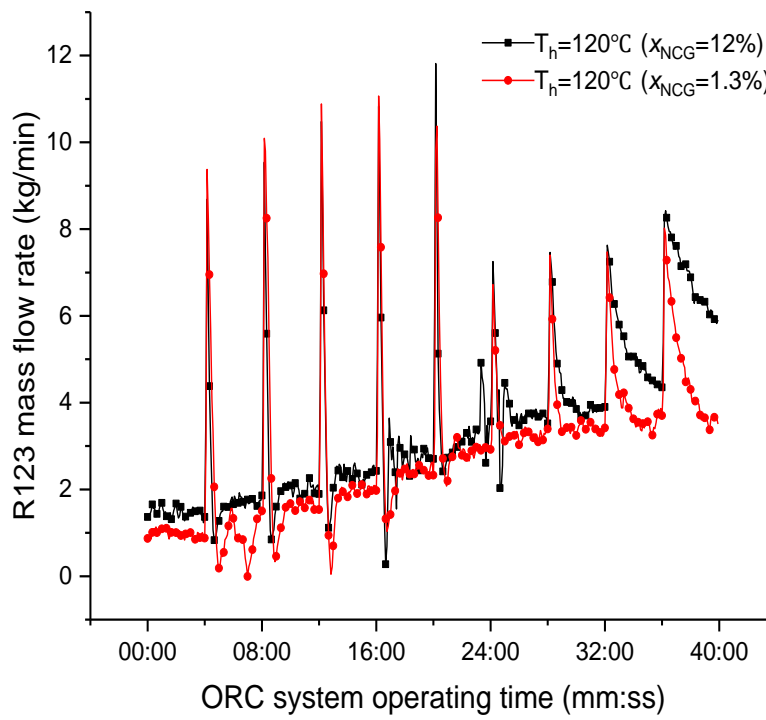
436

437

(b)
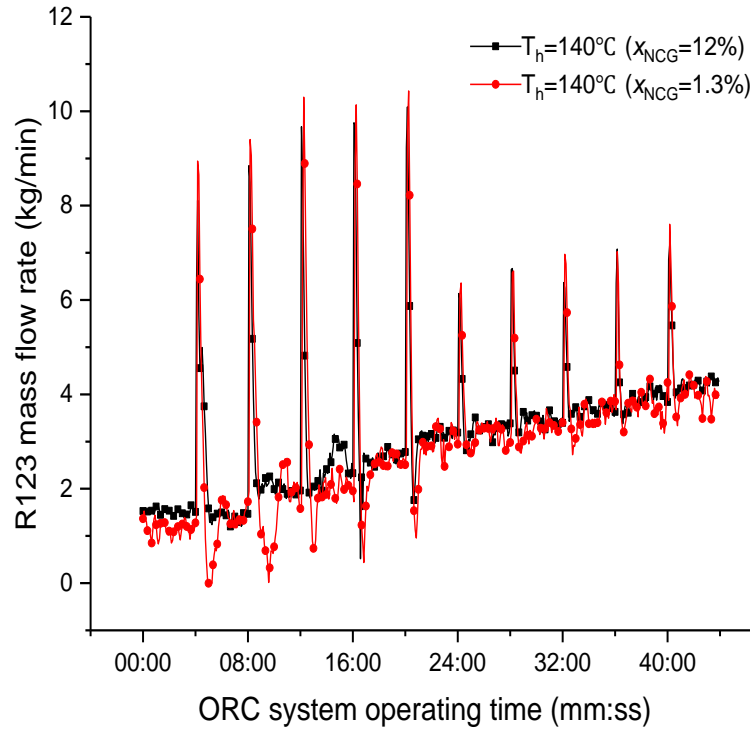
438

439   (c)

440   Fig.12. R123 mass flow rate when T_c=20 °C

441   (a) T_h=100 °C; (b) T_h=120 °C; (c) T_h=140 °C.

442   Fig.13 shows the relative change of electricity output (γ_e), as defined by Eq.(10). At a given

443   time, the pump's input power was the same for the curves, and the rotation speed difference of

444   the expander was generally controlled within 100 rpm for x_{NCG}=12% and x_{NCG}=1.3% as shown

445   in Table 3 and 4. For example, when T_c=20 °C and the frequency of the converter reached the

446   maximum, the rotation speed of the expander were 2078, 2525 and 2686 rpm for x_{NCG}=1.3%

447   at T_h=100, 120 and 140 °C, respectively. And corresponding to 1972, 2548, and 2684 rpm for

448   x_{NCG}=12%.

449   NCGs had direct impact on the operating pressure of the expander, which further

450 influenced the electricity output. At low converter frequency, γ_e was marked owing to the

451 lower RCOPR and higher operating pressure ratio (γ_p) of the expander at x_{NCG}=1.3%, as

452 displayed in Fig.11 and Fig.14. The maximum γ_e was 114% when T_h=100 °C, T_c=50 °C and

453 f=18.5 Hz. On the other hand, γ_e was almost zero or even negative at high converter frequency

454 especially when R123 got near the saturated vapor state. Two reasons can be given. First, when

455 x_{NCG}=1.3%, γ_p was large at high converter frequency. It even reached 12 when T_h=140 °C,

456 T_c=20 °C and f=36.0 Hz. The built-in expansion ratio of the expander was only 3.5. Large γ_p

457 led to highly off-design operation and low efficiency of the expander. Second, the expander

458 was connected with the generator via a big magnetic coupler. A fan was employed to cool down

459 the generator and there was heat transfer from the expander. The heat loss was expected to be

460 significant for this 1 kW expander and hence the expansion process became non-adiabatic.

461 When saturated R123 (or nearly saturated) entered the expander, it was likely to fall into binary

462 phase state due to the heat loss. In fact, binary phase state at the expander outlet had been

463 monitored in some situations. The quality of R123 dropped during expansion, which degraded

464 the performance of the expander. Since lower x_{NCG} was accompanied by larger γ_p, the average

465 quality of R123 should be lower than that with higher x_{NCG}, making the electricity output less.
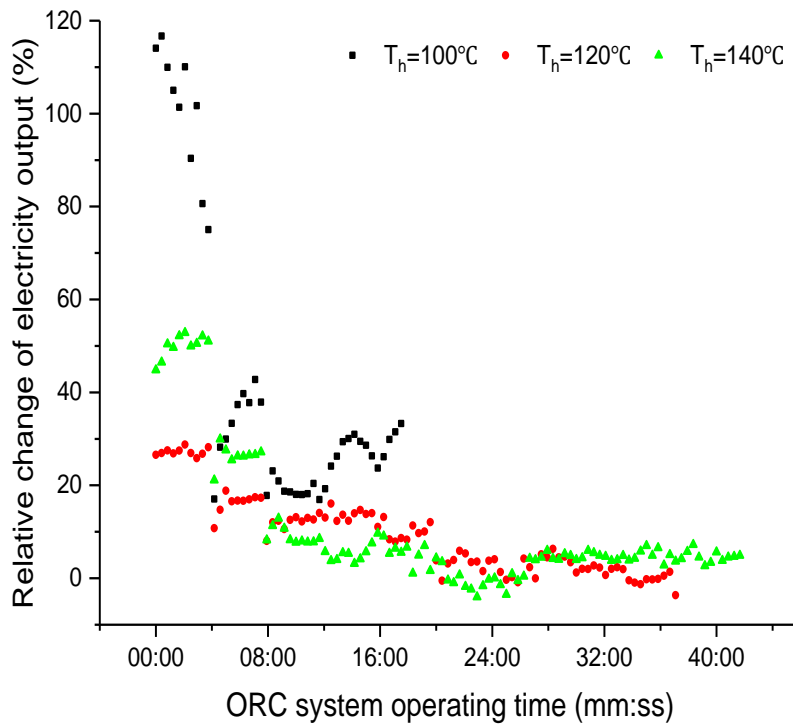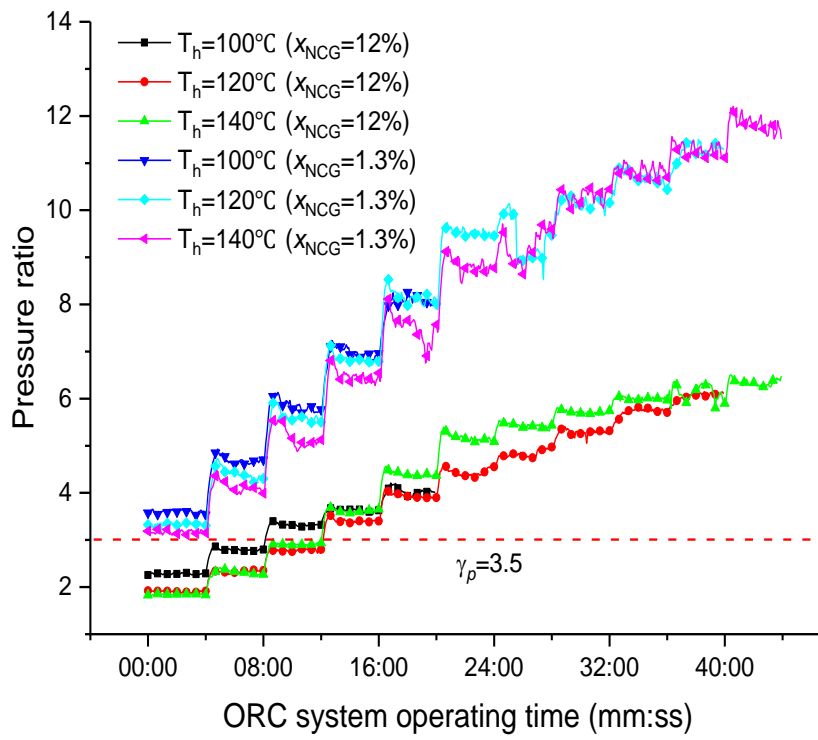
(a)

466

467

(b)

468

469

(c)
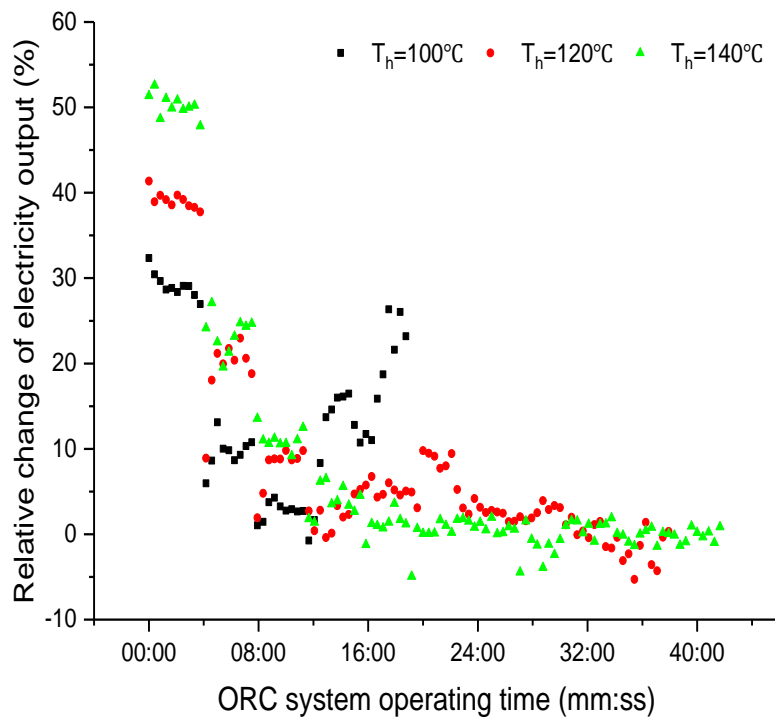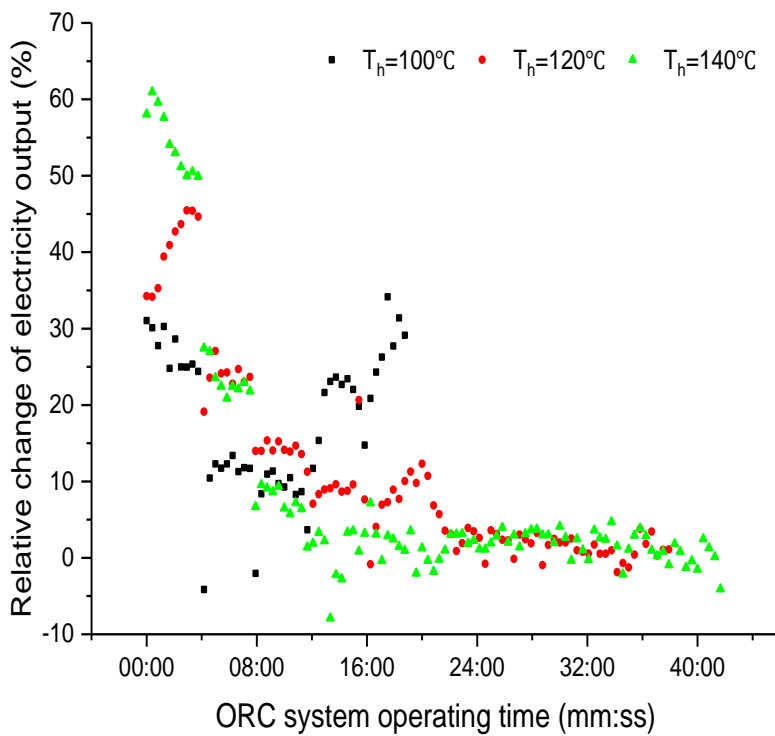
Fig.13. Relative change of electricity output

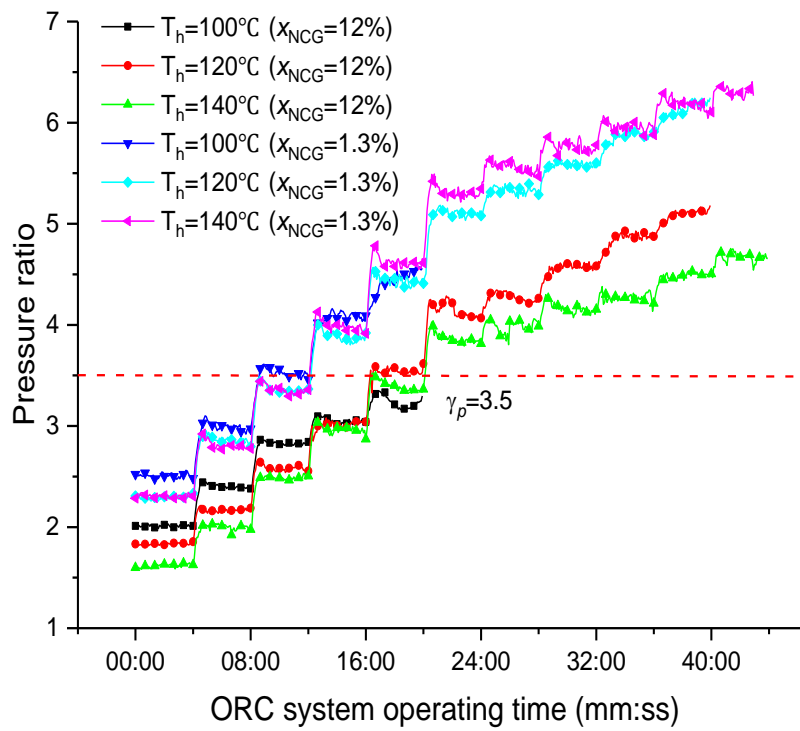(a) T_c=20 °C; (b) T_c=40 °C; (c) T_c=50 °C.

474

475

(a)

476

477

(b)
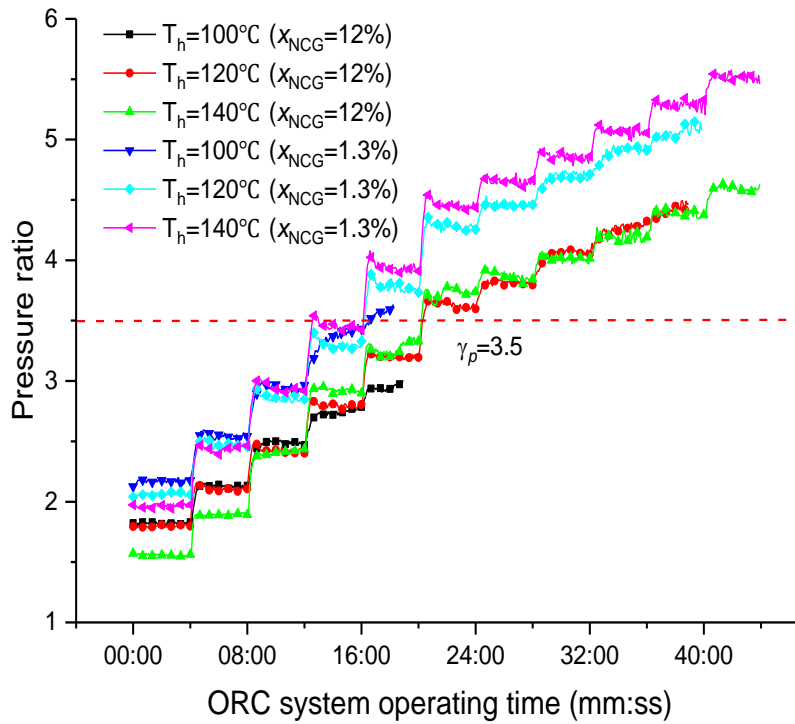
(c)

Fig.14. Variations of pressure ratio of the scroll expander

(a) T_c=20 °C; (b) T_c=40 °C; (c) T_c=50 °C.

5.4 Uncertainty analysis

The expander inlet/outlet pressure and temperature, mass flow rate through pump and generator output were measured directly by the transmitters, thermocouples, flow meter and power meter of accuracy of ±1.0%, ±0.5°C, ±0.15%, ±0.5%, respectively.

The mass fraction of NCGs is determined by Eq.(3). The relative error in x_{NCGs} can be approximately expressed by ER(x_{NCGs})$_\gamma$ ≈ ER(ρ_{R123}/ρ_{NCGs}). As illustrated in Figs.5 and 6, x_{NCGs} of 12% and 1.3% is estimated at temperature of about 11.6 °C and 26.2 °C. With an accuracy of ±0.5°C in thermocouples, the relative error in vapor density of R123 should be ±2.0% and ±1.7%. The relative error in NCGs density should be about ±2.8% and ±15.6%. So ER(x_{NCGs})$_\gamma$

491   at temperature around 11.6 $^{\circ}$C and 26.2 $^{\circ}$C is ±4.8% and ±17.3%. The relative error is large for

492   x_{NCGs}=1.3%. This uncertainty is caused by the low partial pressure of NCGs. It is noteworthy

493   that this paper pays great attention to the mechanism of the ORC performance degradation,

494   rather than the quantitative relationship between the ORC output and x_{NCGs}. The influence of

495   x_{NCGs} on the output is investigated qualitatively. Though error in x_{NCGs} exists, the mechanism

496   should be valid.

497   RCOPR is expressed by Eq.(9). So ER$(RCOPR)_\gamma \approx$ ER$(p_{s,out})$ /$p_{s,out,i}$ + ER$(p_{s,out,i})\times(p_{s,out}$

498   /$p^2_{s,out,i}$). $p_{s,out,i}$ is the ideal backpressure of the expander (i.e. the saturation pressure in the

499   condenser). ER$(p_{s,out})_\gamma$ is ±1.0%, while error in $p_{s,out,i}$ is related to the uncertainty in the

500   condensation temperature.

501   Unlike oil temperature that could be adjusted precisely by the controller, the cooling water

502   temperature was associated with the environment temperature, which fluctuated from time to

503   time. T_c may change during the test. For example, Fig.15 displays the relative variations of T_c

504   when T_h=100, 120 and 140 $^{\circ}$C and x_{NCGs}=1.3%. T_c is around 20 $^{\circ}$C. The relative variation (ΔT)

505   is defined by ΔT=T-T_0 (T_0 is the temperature at 00:00). It falls within ±1 $^{\circ}$C. In further

506   consideration of thermocouple accuracy of ±0.5 $^{\circ}$C, the relative error in the condensation

507   temperature would be ±1.5 $^{\circ}$C. According to R123 properties, ER$(p_{s,out,i})_\gamma$ is about ±4.1%.

508   Therefore, ER$(RCOPR)_\gamma$ is expected to be within ±5.1% when T_c is around 20 $^{\circ}$C. It should

509   be less in the situation of T_c around 40 $^{\circ}$C or 50 $^{\circ}$C because of the higher saturation pressure.

510
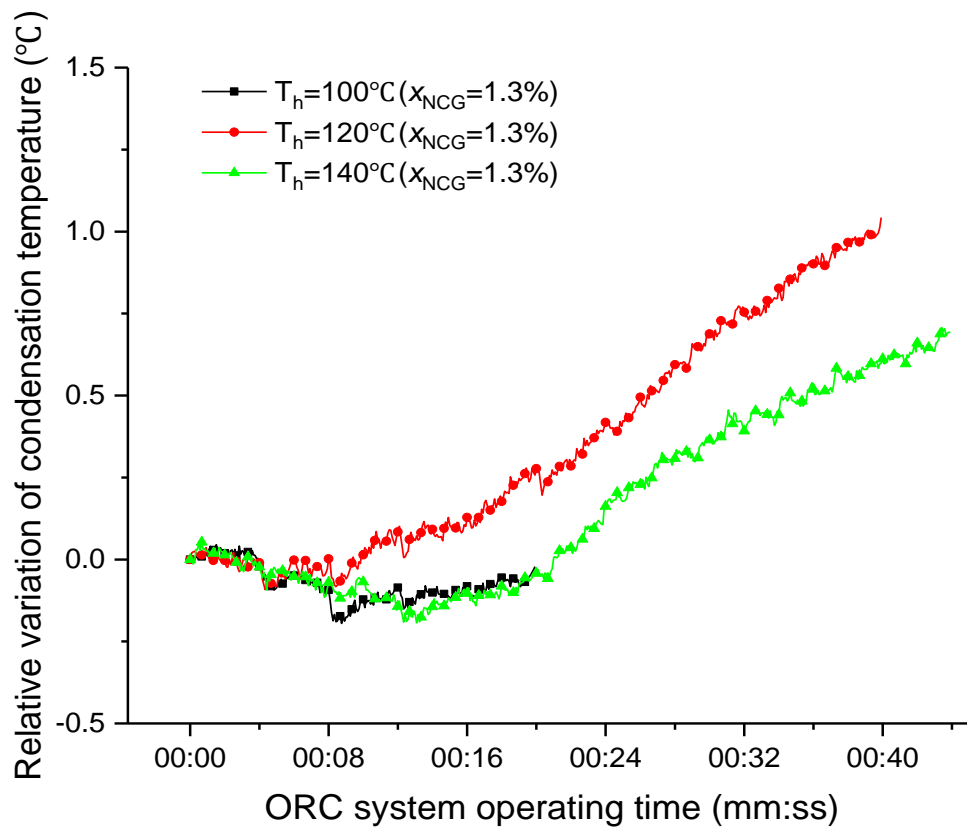
Fig.15. Relative variations of condensation temperature on the conditions of T_h=100, 120 and 140 °C and

x_{NCGs}=1.3%

6. Further discussion

According to the above experiment results, in order to reduce the impacts of NCGs on the

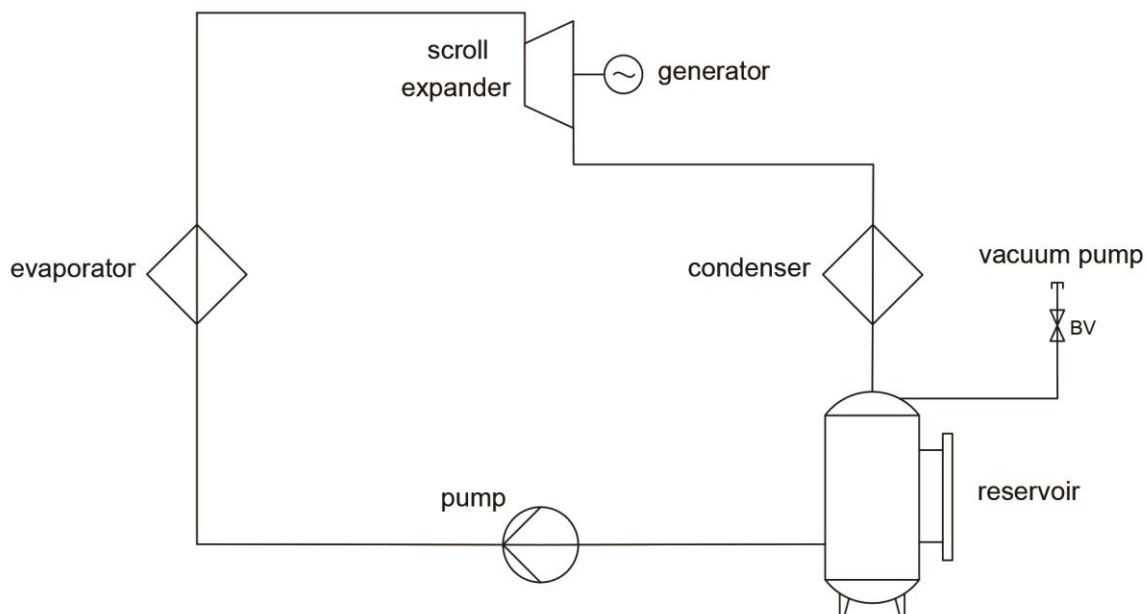condenser outlet pressure and electricity output in ORC system, high FROR should be avoided.

Since NCGs are trapped inside the reservoir, there is an alternative design for NCGs draining,

as illustrated in Fig.15. The vacuum pump is connected with the upper position of reservoir.

After a long time operation of the ORC, the NCGs are expected to be accumulated and the

valves at the reservoir inlet and outlet can be closed. The working fluid in the reservoir is

521 recovered first. Then the vacuum pump works to drain off the NCGs. The design offers a very

522 simple, efficient way of NCGs extraction because the reservoir is far smaller than the whole

523 system and there is not much waste of the ORC fluids.

524

525 Fig.15. Improved ORC system structure

526 **7. Conclusions**

527 In this paper, the effects of NCGs with mass fraction (x_{NCG}) of 12% and 1.3% on the ORC

528 system are studied, especially on the condenser outlet pressure and electricity output on various

529 conditions of hot side temperature (T_h), condensation temperature (T_C) and converter frequency

530 (*f*). The proposed reduced coefficient of pressure ratio (RCOPR) and filling ratio of reservoir

531 (FROR) are helpful for comprehending the mechanism of the NCG-effects. It is obvious that

532 the presence of NCGs in the ORC system changed the condenser outlet pressure directly, and

533 further influenced the electricity output. Through the comparative experiment results, it can be

534   concluded that:

535   (1) The distribution of NCGs can vary. NCGs distributed throughout the pipelines and

536   components when the ORC system was on quasi-steady condition. But the NCGs were

537   squeezed in the reservoir when the ORC system was stably operated, leading to an elevated

538   backpressure of expander. From this viewpoint, a small amount of NCGs still have great

539   possibility to reduce the ORC output.

540   (2) The increments of condenser outlet pressure and RCOPR due to NCGs were more obvious

541   at higher x_{NCG}. Moreover, the condenser outlet pressure and RCOPR were an increasing

542   function with respect to the FROR. A larger FROR was generally accompanied with higher T_h

543   and lower converter frequency.

544   (3) The NCGs had an indirect effect on the electricity output, which was related with both the

545   operating pressure ratio and off-design characteristics of the expander. The electricity with x_{NCG}

546   =1.3% exceeded that with x_{NCG}=12% by 114% when T_h=100 °C, T_c=50 °C and f=18.5 Hz. The

547   increment of electricity output was less appreciable when the expander underwent highly off-

548   design conditions, which was reached as f>31.0 Hz.

549   **Acknowledgment**

554   Innovative Research Team Program (2014607101008).

555   **References**

556   [1] Tchanche BF, Lambrinos G, Frangoudakis A, Papadakis G. Low-grade heat conversion

557   into power using organic Rankine cycles – A review of various applications. Renewable and

558   Sustainable Energy Reviews. 2011;15:3963-79.

559   [2] Bao JJ, Zhao L. A review of working fluid and expander selections for organic Rankine

560   cycle. Renewable & Sustainable Energy Reviews. 2013;24:325-42.

561   [3] Chen HJ, Goswami DY, Stefanakos EK. A review of thermodynamic cycles and working

562   fluids for the conversion of low-grade heat. Renewable & Sustainable Energy Reviews.

563   2010;14:3059-67.

564   [4] Pu WH, Yue C, Han D, He WF, Liu X, Zhang Q, et al. Experimental study on Organic

565   Rankine cycle for low grade thermal energy recovery. Applied Thermal Engineering.

566   2016;94:221-7.

567   [5] Cho SY, Cho CH, Choi SK. Experiment and cycle analysis on a partially admitted axial-

568   type turbine used in the organic Rankine cycle. Energy. 2015;90:643-51.

569   [6] Kang SH. Design and experimental study of ORC (organic Rankine cycle) and radial

570   turbine using R245fa working fluid. Energy. 2012;41:514-24.

571   [7] Chang JC, Hung TC, He YL, Zhang WP. Experimental study on low-temperature organic

572   Rankine cycle utilizing scroll type expander. Applied Energy. 2015;155:150-9.

573   [8] Declaye S, Quoilin S, Guillaume L, Lemort V. Experimental study on an open-drive scroll

expander integrated into an ORC (Organic Rankine Cycle) system with R245fa as working

fluid. Energy. 2013;55:173-83.

[9] Quoilin S, Lemort V, Lebrun J. Experimental study and modeling of an Organic Rankine

Cycle using scroll expander. Applied Energy. 2010;87:1260-8.

[10] Desideri A, Gusev S, van den Broek M, Lemort V, Quoilin S. Experimental comparison

of organic fluids for low temperature ORC (organic Rankine cycle) systems for waste heat

recovery applications. Energy. 2016;97:460-9.

[11] Zhang YQ, Wu YT, Xia GD, Ma CF, Ji WN, Liu SW, et al. Development and experimental

study on organic Rankine cycle system with single-screw expander for waste heat recovery

from exhaust of diesel engine. Energy. 2014;77:499-508.

[12] Zheng N, Zhao L, Wang XD, Tan YT. Experimental verification of a rolling-piston

expander that applied for low-temperature Organic Rankine Cycle. Applied Energy.

2013;112:1265-74.

[13] Qiu GQ, Shao YJ, Li JX, Liu H, Riffat SB. Experimental investigation of a biomass-fired

ORC-based micro-CHP for domestic applications. Fuel. 2012;96:374-82.

[14] Peris B, Navarro-Esbri J, Moles F, Mota-Babiloni A. Experimental study of an ORC

(organic Rankine cycle) for low grade waste heat recovery in a ceramic industry. Energy.

2015;85:534-42.

[15] Eyerer S, Wieland C, Vandersickel A, Spliethoff H. Experimental study of an ORC

(Organic Rankine Cycle) and analysis of R1233zd-E as a drop-in replacement for R245fa for

low temperature heat utilization. Energy. 2016;103:660-71.

595   [16] Jung H-C, Taylor L, Krumdieck S. An experimental and modelling study of a 1 kW

596   organic Rankine cycle unit with mixture working fluid. Energy. 2015;81:601-14.

597   [17] Bamorovat Abadi G, Yun E, Kim KC. Experimental study of a 1 kw organic Rankine

598   cycle with a zeotropic mixture of R245fa/R134a. Energy. 2015;93:2363-73.

599   [18] Kosmadakis G, Manolakos D, Papadakis G. Experimental investigation of a low-

600   temperature organic Rankine cycle (ORC) engine under variable heat input operating at both

601   subcritical and supercritical conditions. Applied Thermal Engineering. 2016;92:1-7.

602   [19] Yun E, Kim D, Yoon SY, Kim KC. Experimental investigation of an organic Rankine

603   cycle with multiple expanders used in parallel. Applied Energy. 2015;145:246-54.

604   [20] Gao P, Wang LW, Wang RZ, Jiang L, Zhou ZS. Experimental investigation on a small

605   pumpless ORC (organic rankine cycle) system driven by the low temperature heat source.

606   Energy. 2015;91:324-33.

607   [21] Peris B, Navarro-Esbrí J, Molés F, González M, Mota-Babiloni A. Experimental

608   characterization of an ORC (organic Rankine cycle) for power and CHP (combined heat and

609   power) applications from low grade heat sources. Energy. 2015;82:269-76.

610   [22] Manolakos D, Kosmadakis G, Kyritsis S, Papadakis G. On site experimental evaluation

611   of a low-temperature solar organic Rankine cycle system for RO desalination. Solar Energy.

612   2009;83:646-56.

613   [23] Tian H, Chang L, Gao Y, Shu G, Zhao M, Yan N. Thermo-economic analysis of zeotropic

614   mixtures based on siloxanes for engine waste heat recovery using a dual-loop organic Rankine

615   cycle (DORC). Energy Conversion and Management. 2017;136:11-26.

616 [24] Eveloy V, Rodgers P, Qiu LY. Performance investigation of a power, heating and seawater

617 desalination poly-generation scheme in an off-shore oil field. Energy. 2016;98:26-39.

618 [25] Lecompte S, Huisseune H, van den Broek M, De Paepe M. Methodical thermodynamic

619 analysis and regression models of organic Rankine cycle architectures for waste heat recovery.

620 Energy. 2015;87:60-76.

621 [26] Fernandez FJ, Prieto MM, Suarez I. Thermodynamic analysis of high-temperature

622 regenerative organic Rankine cycles using siloxanes as working fluids. Energy. 2011;36:5239-

623 49.

624 [27] Li J, Alvi JZ, Pei G, Ji J, Li PC, Fu HD. Effect of working fluids on the performance of a

625 novel direct vapor generation solar organic Rankine cycle system. Applied Thermal

626 Engineering. 2016;98:786-97.

627 [28] He J, Miao J, Bai L, Lin G, Zhang H, Wen D. Effect of non-condensable gas on the startup

628 of a loop heat pipe. Applied Thermal Engineering. 2016.

629 [29] Singh R, Akbarzadeh A, Mochizuki M. Operational characteristics of the miniature loop

630 heat pipe with non-condensable gases. International Journal of Heat and Mass Transfer.

631 2010;53:3471-82.

632 [30] Dube V, Akbarzadeh A, Andrews J. The effects of non-condensable gases on the

633 performance of loop thermosyphon heat exchangers. Applied Thermal Engineering.

634 2004;24:2439-51.

635 [31] Sapienza A, Frazzica A, Freni A, Aristov Y. Dramatic effect of residual gas on dynamics

636 of isobaric adsorption stage of an adsorptive chiller. Applied Thermal Engineering.

637   2016;96:385-90.

638   [32] Cecchinato L, Dell'Eva M, Fornasieri E, Marcer M, Monego O, Zilio C. The effects of

639   non-condensable gases in domestic appliances. Int J Refrig. 2007;30:19-27.

640   [33] Li XF, Li MX, Ma YT, Yan QH. The influence of nitrogen on an expander in a carbon

641   dioxide transcritical heat pump. Applied Thermal Engineering. 2013;59:182-8.

642   [34] Hua T, Yitai M, Minxia L, Haiqing G, Zhongyan L. Influence of a non-condensable gas

643   on the performance of a piston expander for use in carbon dioxide trans-critical heat pumps.

644   Applied Thermal Engineering. 2011;31:1943-9.

645   [35] Fu W, Li XW, Wu XX, Corradini ML. Numerical investigation of convective

646   condensation with the presence of non-condensable gases in a vertical tube. Nuclear

647   Engineering and Design. 2016;297:197-207.

648   [36] Berrichon JD, Louahlia-Gualous H, Bandelier P, Bariteau N. Experimental and theoretical

649   investigations on condensation heat transfer at very low pressure to improve power plant

650   efficiency. Energy Conversion and Management. 2014;87:539-51.

651   [37] Huang J, Zhang JX, Wang L. Review of vapor condensation heat and mass transfer in the

652   presence of non-condensable gas. Applied Thermal Engineering. 2015;89:469-84.

653   [38] Yin Z, Wen JJ, Wu YN, Wang QW, Zeng M. Effect of non-condensable gas on laminar

654   film condensation of steam in horizontal minichannels with different cross-sectional shapes.

655   International Communications in Heat and Mass Transfer. 2016;70:127-31.

656   [39] Chen CK, Lin YT. Turbulent film condensation in the presence of non-condensable gases

657   over a horizontal tube. International Journal of Thermal Sciences. 2009;48:1777-85.

658   [40] Mukhopadhyay S, Som SK, Chakraborty S. A generalized mathematical description for

659   comparative assessment of various horizontal polar tube geometries with regard to external

660   film condensation in presence of non-condensable gases. International Journal of Heat and

661   Mass Transfer. 2007;50:3437-46.

662   [41] Ma XH, Zhou XD, Lan Z, Li YM, Zhang Y. Condensation heat transfer enhancement in

663   the presence of non-condensable gas using the interfacial effect of dropwise condensation.

664   International Journal of Heat and Mass Transfer. 2008;51:1728-37.

665   [42] Tanner DW, Pope D, Potter CJ, West D. Heat transfer in dropwise condensation at low

666   steam pressures in the absence and presence of non-condensable gas. International Journal of

667   Heat and Mass Transfer. 1968;11:181-90.

668   [43] Tanner DW, Potter CJ, Pope D, West D. Heat transfer in dropwise condensation—Part I

669   The effects of heat flux, steam velocity and non-condensable gas concentration. International

670   Journal of Heat and Mass Transfer. 1965;8:419-26.

671   [44] Yi QJ, Tian MC, Yan WJ, Qu XH, Chen XB. Visualization study of the influence of non-

672   condensable gas on steam condensation heat transfer. Applied Thermal Engineering.

673   2016;106:13-21.

674   [45] Dharma Rao V, Murali Krishna V, Sharma KV, Rao PVJM. Convective condensation of

675   vapor in the presence of a non-condensable gas of high concentration in laminar flow in a

676   vertical pipe. International Journal of Heat and Mass Transfer. 2008;51:6090-101.

677   [46] Groff MK, Ormiston SJ, Soliman HM. Numerical solution of film condensation from

678   turbulent flow of vapor–gas mixtures in vertical tubes. International Journal of Heat and Mass

679   Transfer. 2007;50:3899-912.

680   [47] Som SK, Chakraborty S. Film condensation in presence of non-condensable gases over

681   horizontal tubes with progressively increasing radius of curvature in the direction of gravity.

682   International Journal of Heat and Mass Transfer. 2006;49:594-600.

683   [48] Denny VE, Jusionis VJ. Effects of Noncondensable Gas and Forced Flow on Laminar

684   Film Condensation. International Journal of Heat and Mass Transfer. 1972;15:315-&.

685   [49] Chantana C, Kumar S. Experimental and theoretical investigation of air-steam

686   condensation in a vertical tube at low inlet steam fractions. Applied Thermal Engineering.

687   2013;54:399-412.

688   [50] Gu HF, Chen Q, Wang HJ, Zhang HQ. Condensation of a hydrocarbon in the presence of

689   a non-condensable gas: Heat and mass transfer. Applied Thermal Engineering. 2015;91:938-

690   45.

691   [51] Omidvarborna H, Mehrabani-Zeinabad A, Esfahany MN. Effect of electrohydrodynamic

692   (EHD) on condensation of R-134a in presence of non-condensable gas. International

693   Communications in Heat and Mass Transfer. 2009;36:286-91.

694   [52] Battino R, Rettich TR, Tominaga T. The Solubility of Nitrogen and Air in Liquids. Journal

695   of Physical and Chemical Reference Data. 1984;13:563-600.

696   [53] Fischer K, Wilken M. Experimental determination of oxygen and nitrogen solubility in

697   organic solvents up to 10 MPa at temperatures between 298 K and 398 K. J Chem Thermodyn.

698   2001;33:1285-308.

699   [54] R123 Safety Data Sheet. National Refrigerants.Inc; 2015.

700